Received: Added at production | Revised: Added at production | Accepted: Added at production

DOI: xxx/xxxx

ARTICLE TYPE

# High-order isogeometric modified method of characteristics for two-dimensional coupled Burgers' equations

Ilham Asmouh[1,4] | Mofdi El-Amrani[2] | Mohammed Seaid[3] | Naji Yebari[4]

[1]International Water Research Institute, University Mohammed VI Polytechnic, Benguerir, Morocco

[2]Dpto. Matemáticas Applicada, Ciencia e Ingeniería de Materiales y Tecnología Electrónica, Universidad Rey Juan Carlos, 28933 Móstoles-Madrid, Spain

[3]Department of Engineering, University of Durham, South Road, Durham DH1 3LE, UK

[4]Department of Mathematics, Faculty of Sciences, University Abdelmalek Essaadi, Tetouan, Morocco

**Correspondence**

*Mofdi El-Amrani Email: mofdi.elamrani@urjc.es

**Summary**

This paper presents a novel isogeometric modified method of characteristics for the numerical solution of the two-dimensional nonlinear coupled Burgers' equations. The method combines the modified method of characteristics and the high-order NURBS (non-uniform rational B-splines) elements to discretize the governing equations. The Lagrangian interpretation in this isogeometric analysis greatly reduces the time truncation errors in the Eulerian methods. A third-order explicit Runge-Kutta scheme is used for the discretization in time. We present a detailed description of the algorithm used for the calculation of departure points and the interpolation stage. Our focus is on constructing highly accurate and stable solvers for the two-dimensional nonlinear coupled Burgers' equations at high Reynolds numbers. A variety of benchmark tests and numerical examples are provided to show the effectiveness, accuracy, and performance of the proposed modified method of characteristics by virtue of potential advantages of isogeometric analysis. The method developed is anticipated to provide new research directions to the practical calculation of incompressible flows and to studies of their physical behavior.

**KEYWORDS:**

Isogeometric analysis; Modified method of characteristics; Burgers' equations; NURBS basis functions.

## 1 | INTRODUCTION

In general, convection-dominated viscous flows are characterized by some complicated features such as boundary layers which involve very strong gradients. As a consequence, the formulation of a highly accurate computational analysis requires the adjustment of the local scale difference between convection and diffusion terms. The standard Galerkin formulation has been used for the treatment of such problems, but exhibits spurious instabilities, see for example [1]. Unfortunately, this carries over the isogeometric counterpart approach as well. To handle this problem, several numerical methods have been introduced including the well-known Streamline-upwind Petrov-Galerkin (SUPG) methods. The idea of SUPG methods is to increase the numerical stability without degrading the accuracy by insertion of residual-based modification of the Galerkin method. Authors in [2] proposed a SUPG-stabilized isogeometric analysis with reduced order for solving the unsteady convection-dominated diffusion reaction problems. For the time discretization, authors in [2] used the Crank-Nicholson scheme which is unconditionally stable but requires

small time steps in order to achieve high accuracy. Similar ideas were proposed in [3] for steady convection-diffusion problems. In [4], a space-time isogeometric analysis is proposed for parabolic equations in fixed and moving spatial computational domains. Authors in [5] have presented a numerical study based on finite elements and B-splines for one-dimensional advection-diffusion problems. The isogeometric analysis has also been used in [6] for elliptic boundary-value problems with singular parameterizations. In [7], an isogeometric analysis with direction splitting has been investigated for non-stationary advection-diffusion problems. In each space direction, a stabilized mixed method based on the residual minimization is used. Preconditioning immersed isogeometric finite element methods have also been studied in [8] by investigating the conditioning analysis of immersed finite element methods for systems that are not symmetric positive definite, but the study is redirected to parabolic problems and steady Navier-stokes equations. A class of algebraic flux correction procedures has been proposed in [9] to overcome the spurious oscillatory behavior appeared in the solutions of compressible flows problems. Authors in [10] have also suggested to use tensioned splines instead of NURBS or B-splines in order to reduce the non-physical oscillations for a class of steady advection-diffusion problems. For incompressible flows, the isogeometric analysis has been investigated in many works, see for instance [11,12,13,14,15,16,17].

In this paper, given a two-dimensional bounded domain $\Omega \subset \mathbb{R}^2$ with Lipschitz boundary $\Gamma$ and a given time interval $[0, T]$, we are interested in solving the two-dimensional unsteady nonlinear coupled Burgers' equations

$$\frac{\partial \boldsymbol{u}}{\partial t} + \boldsymbol{u} \cdot \nabla \boldsymbol{u} - \frac{1}{Re} \Delta \boldsymbol{u} = \boldsymbol{0}, \tag{1}$$

where $\boldsymbol{u} = (u, v)^\top$ the velocity field, $u$ the velocity in $x$-direction, $v$ the velocity in $y$-direction, and $Re$ the Reynolds number. Note that this nondimensional number is usually used to control the relative importance of convection compared to diffusion in (1). To provide a well-posed mathematical problem, equations (1) are equipped with suitable boundary and initial conditions. In general, it is challenging to solve this type of equations for small values of diffusion which correspond to high Reynolds numbers. In this case, the solution usually exhibits sharp gradients due to the formation of thin boundary layers in the computational domain. Another challenge is the nonlinear nature of the problem which makes most conventional finite element methods not a good choice as most of these methods require a linearization of the problem at each time step. Many research works have been published in the literature to treat the nonlinear viscous Burgers equations. For example, a fourth-order numerical algorithm based on the two-dimensional Hopf-Cole transformation to solve the system of two-dimensional Burgers' equations with relatively large Reynolds numbers has been presented in [18]. The Hopf-Cole transformation allows to avoid any linearization of the equations as this transforms the problem to a class of linear heat equations. The resulting system is then solved using a forth-order finite difference scheme. To maintain the forth-order accuracy, authors apply a Richardsons extrapolation for time discretization. Apparently the main drawback in this work, is the extension to complex geometries since the authors adopt a finite difference scheme to discretize the space. In [19], the authors adopt the same Hopf-Cole transformation and use the spectral volume (SV) method to discretize the spacial derivatives. In this case, no need to Richardsons extrapolation as the high-order accuracy is guaranteed by the SV method. Apparently, a serious weakness with this argument, however, is the necessity to approximate the initial and boundary conditions via a quadrature rule which may create accumulation of errors. Authors in [20] have also presented a MacCormack approach which can be interpreted as a predictor-corrector formulation to solve the two-dimensional coupled Burgers' equations. This method is powerful for small Reynolds numbers but it is only second-order accurate in time and space for large Reynolds numbers. In [21], a time splitting operator has been proposed to separate the nonlinear advection part from the diffusion part in the two-dimensional coupled Burgers' equations. The nonlinear part is linearized based on a special Taylor-expansion approach whereas, the diffusion part is discretized using a finite element method. As in previous works, the values of Reynolds number used are relatively small (up to $Re = 100$).

The main limitation of most of the previous works is the use of Eulerian-based discretizations which require small time steps in order to achieve both numerical stability and the desired accuracy. As a result, the computational cost is increased, especially for long-term flow simulations. Furthermore, some works have tended to focus on transport problems with linear, smooth and constant velocity fields. The focus of the current study is on the numerical solution of highly convection-dominated problems with nonlinear convection. In general, convective terms are recognized as being sources of oscillations, especially when the velocity field exhibits sharp gradient. To deal with this problem, we suggest to treat the convective part by the modified method of characteristics in which the non-uniform rational B-spline (NURBS) functions are used to interpolate the solution from previous time steps. By doing so, no linearization procedures are required for the two-dimensional coupled Burgers' equations (1). Moreover, the main feature of modified method of characteristics is the ability to use large time steps in the simulations while maintaining stability. This make this scheme an attractive choice for long-term flow simulations. The accuracy of the proposed isogeometric modified method of characteristics is attributed to two facts: the first one is attributed to the reduced computational

cost which is a powerful key of a Lagrangian-based method compared to its Eulerian counterpart, whereas the second one is related to the NURBS basis functions used for space discretization. To increase the accuracy, we interpolate the solution using high-order NURBS basis functions in the isogeometric analysis framework. For the space discretization, we implement an isogeometric finite element approach. The main contribution in this work is using the NURBS functions to interpolate the solution from previous time step using an $L^2$-projection procedure introduced in [22,23]. The idea behind the $L^2$-projection approach consists of evaluating the solution at the departure points using a set of quadrature points distributed in the host patch. Thus, we combine both main advantages of the modified method of characteristics related to the use of large time steps and the ability of isogeometric analysis in preserving the geometry exact, no matter how much the mesh is coarse. Notice that the computational treatment of the complex patterns resulting from dominated convection terms often requires efficient numerical algorithms with high regularity. These advantages are achieved in the present work by using the $k$-refinement strategy which is unique to isogeometric analysis and do not have analogue in conventional finite element methods. This approach offers high inter-element continuity and the method has a potential approach to high-precision analysis over the standard $p$-refinement strategies, see [24,25] among others. The performance of the proposed isogeometric modified method of characteristics is demonstrated for several test examples of the two-dimensional coupled Burgers' equations. To the best of our knowledge, combining an isogeometric analysis and the modified method of characteristics for solving the nonlinear Burgers equations is proposed for the first time.

This paper is organized as follows. In section 2 we introduce tools used for the NURBS-based isogeometric analysis. Formulation of the isogeometric modified method of characteristics for solving the two-dimensional coupled Burgers' equations is presented in section 3. This section includes the calculation of departure points, the NURBS-based procedure for the convection stage and an explicit third-order Runge-Kutta scheme to solve the diffusion stage. Section 4 is devoted to numerical results for several examples of two-dimensional unsteady nonlinear coupled Burgers' equations. Our new approach is demonstrated to enjoy the expected efficiency as well as the accuracy. Concluding remarks are summarized in section 5.

## 2 | NURBS-BASED ISOGEOMETRIC ANALYSIS

In this section a brief overview of the IsoGeometric Analysis (IGA) is presented and more details on IGA can be found in [25,26,24,27] among others. This includes the NURBS basis functions and the IGA space on which the approximate solution is defined. Thus, given a knot vector $\Xi$ which is defined as an ordered set of increasing parameter values $\Xi = \left\{\xi_1, \xi_2, \ldots, \xi_{m_b+p+1}\right\}$, where $m_b$ denotes the number of basis functions and $p$ is the polynomial order, the associated set of B-spline basis functions $\left\{N_i^p\right\}_{i=1}^{m_b}$ are defined recursively by the Cox-de-Boor formula as follows [25,26]:

Starting with the following zeroth-order basis function ($p = 0$)

$$N_i^0(\xi) = \begin{cases} 1, & \text{if} \quad \xi_i \leqslant \xi \leqslant \xi_{i+1}, \quad i = 1, \ldots, m_b, \\ \\ 0, & \text{elsewhere}, \end{cases} \tag{2}$$

the B-spline basis function of an order $p \geqslant 1$ is defined by

$$N_i^p(\xi) = \frac{\xi - \xi_i}{\xi_{i+p} - \xi_i} N_i^{p-1}(\xi) + \frac{\xi_{i+p+1} - \xi}{\xi_{i+p+1} - \xi_{i+1}} N_{i+1}^{p-1}(\xi). \tag{3}$$

The first-order derivative of the B-spline basis function is also computed recursively from the lower order basis functions as

$$\frac{d}{d\xi} N_i^p(\xi) = \frac{p}{\xi_{i+p} - \xi_i} N_i^{p-1}(\xi) + \frac{p}{\xi_{i+p+1} - \xi_{i+1}} N_{i+1}^{p-1}(\xi). \tag{4}$$

In the case of NURBS, the basis functions are derived from B-splines and defined as

$$R_i^p(\xi) = \frac{N_i^p(\xi)\omega_i}{W(\xi)}, \tag{5}$$

where $\left\{N_i^p\right\}_{i=1}^{m_b}$ is the set of B-spline basis functions of order $p$, $\left\{\omega_i\right\}_{i=1}^{m_b}$ is the set of NURBS weights and

$$W(\xi) = \sum_{i=1}^{m_b} N_i^p(\xi)\omega_i,$$

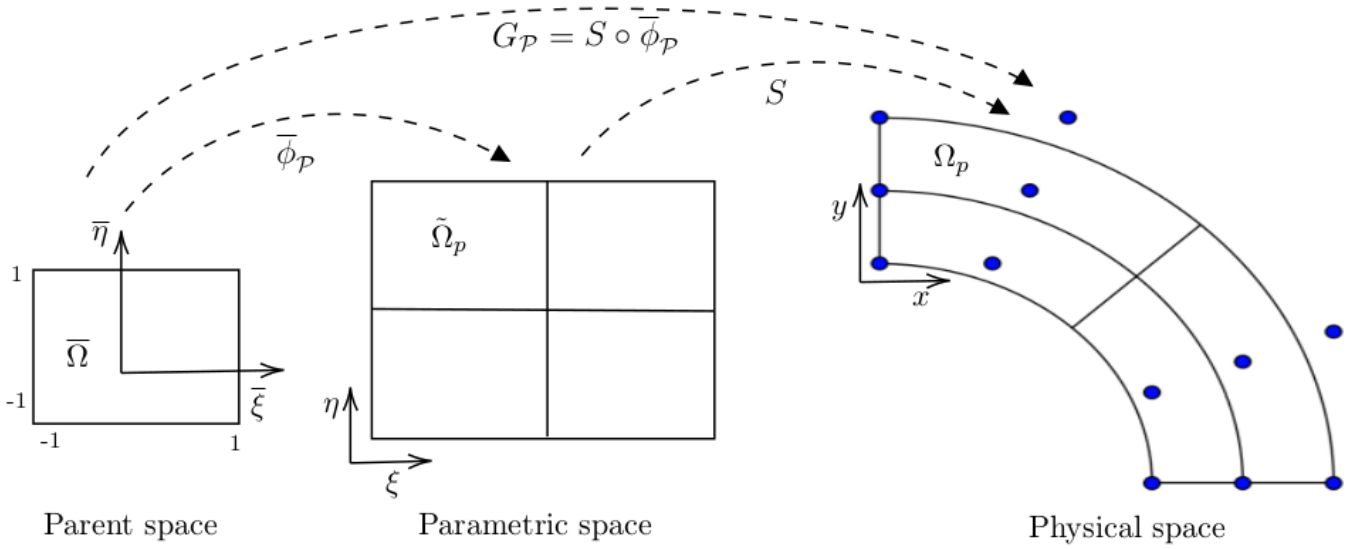


**FIGURE 1** Illustration of mappings from parent space through the parametric space to the physical space.

The first-order derivative of a NURBS basis function $R_i^p$ is obtained using the quotient rule as

$$\frac{d}{d\xi}R_i^p(\xi) = \omega_i \frac{(N_i^p)'(\xi)W(\xi) - N_i^p(\xi)W'(\xi)}{W(\xi)^2}, \tag{6}$$

where $(N_i^p)'(\xi) = \dfrac{d}{d\xi}N_i^p(\xi)$ and $W'(\xi) = \displaystyle\sum_{i=1}^{m_b}(N_i^p)'(\xi)w_i$. The NURBS curves are constructed by a linear combination of NURBS $R_i^p(\xi)$ as

$$C(\xi) = \sum_{i=1}^{m_b} R_i^p(\xi)B_i, \tag{7}$$

where $B_i$ is the vector of control points with $i = 1, \ldots, m_b$. In the same manner, the NURBS surfaces are straightforwardly constructed by considering the tensor product of two NURBS functions $R_i^p(\xi)$ and $R_i^q(\eta)$ as

$$S(\xi,\eta) = \sum_{i=1}^{m_b}\sum_{j=1}^{l_b} R_i^p(\xi)R_j^q(\eta)B_{i,j}, \tag{8}$$

where $B_{i,j}$ is the vector of control points with $i = 1, \ldots, m_b$ and $j = 1, \ldots, l_b$. Here, $m_b$ and $l_b$ denote the total numbers of control points in $x$-direction and $y$-direction, respectively. Note that (8) can also be rewritten in a compact form as

$$S(\xi,\eta) = \sum_{m=1}^{\mathrm{DoF}} R_m^{p,q}(\xi,\eta)B_m, \tag{9}$$

where $R_m^{p,q}$ is the basis function defined as $R_m^{p,q}(\xi,\eta) = R_i^p(\xi)R_j^q(\eta)$ and $\mathrm{DoF} = m_b \times l_b$ is the total number of control points.

Following the same procedure carried out in the conventional finite element analysis, each parent space is mapped to the master space where all IGA computations are performed, see for instance[25] and further details are therein. Thus, the construction of NURBS as a basis function in a discretization framework requires the introduction of the parametric space which is absent in the conventional finite element analysis. This would require an additional mapping to operate in the coordinates of the parent space. An illustration of these two mappings is depicted in Figure 1 where $\overline{\phi}_{\mathcal{P}} : \overline{\Omega} \longrightarrow \widetilde{\Omega}_{\mathcal{P}}$ is the mapping from the parent space to the parametric space, and $S : \widetilde{\Omega}_{\mathcal{P}} \longrightarrow \Omega_{\mathcal{P}}$ is the mapping from the parametric space to the physical space. Note that the mapping $G_{\mathcal{P}} : \overline{\Omega} \longrightarrow \Omega_{\mathcal{P}}$ is given by the composition $S \circ \overline{\phi}_{\mathcal{P}}$. In case of the two-dimensional space, a patch $\widetilde{\Omega}_{\mathcal{P}} = [\xi_i, \xi_{i+1}] \bigotimes [\eta_i, \eta_{i+1}]$ is mapped from the parent space to the parametric space using

$$\overline{\phi}_{\mathcal{P}}(\overline{\xi},\overline{\eta}) = \left(\frac{1}{2}\Big((\xi_{i+1}-\xi_i)\overline{\xi} + (\xi_{i+1}-\xi_i)\Big), \frac{1}{2}\Big((\eta_{j+1}-\eta_j)\overline{\eta} + (\eta_{j+1}-\eta_j)\Big)\right)^{\top}. \tag{10}$$

The determinant of the Jacobian associated with this mapping is given by

$$\left|J^{\bar{\xi},\bar{\eta}}\right| = \frac{1}{4}\left(\xi_{i+1} - \xi_i\right)\left(\eta_{i+1} - \eta_i\right), \tag{11}$$

Similarly, the mapping from the parametric space to the physical space in one- and two-dimensional problems is given by (7) and (8), respectively. In the case of two-dimensional problems, the determinant of the Jacobian associated with this mapping is defined as

$$\left|J^{\xi,\eta}\right| = \frac{\partial x}{\partial \xi}\frac{\partial y}{\partial \eta} - \frac{\partial x}{\partial \eta}\frac{\partial y}{\partial \xi}, \tag{12}$$

with

$$\frac{\partial x}{\partial \xi} = \sum_{i=1}^{m_b} B_i \frac{\partial R_i^p(\xi)}{\partial \xi}, \qquad \frac{\partial x}{\partial \eta} = \sum_{j=1}^{l_b} B_j \frac{\partial R_j^q(\eta)}{\partial \eta}, \qquad \frac{\partial y}{\partial \xi} = \sum_{i=1}^{m_b} B_i \frac{\partial R_i^p(\xi)}{\partial \xi}, \qquad \frac{\partial y}{\partial \eta} = \sum_{j=1}^{l_b} B_j \frac{\partial R_j^q(\eta)}{\partial \eta}.$$

Note that the mapping $G_{\mathcal{P}} : \overline{\Omega} \longrightarrow \Omega_{\mathcal{P}}$ given by the composition $S \circ \bar{\phi}_{\mathcal{P}}$ can straightforwardly be written as follows

$$G_{\mathcal{P}}^{p,q}(\bar{\xi},\bar{\eta}) = \left(\sum_{m=1}^{\mathrm{DoF}} B_m R_m^{p,q}\left(\overline{\phi}_{\mathcal{P}}\left(\bar{\xi},\bar{\eta}\right)\right)\right)\Bigg|_{\mathcal{P}}, \tag{13}$$

where the expression $(\cdot)\Big|_{\mathcal{P}}$ refers to the restriction in the element $\mathcal{P}$. The determinant of the Jacobian associated with this mapping is given by

$$|J| = \left|J^{\xi,\eta}\right|\left|J^{\bar{\xi},\bar{\eta}}\right|. \tag{14}$$

Using the mappings and their associated Jacobians defined above, the integral of a given generic function $f : \Omega \to \mathbb{R}$ in the physical space $\Omega$ is obtained as

$$\begin{aligned}
\int_{\Omega} f(\boldsymbol{x})\, d\Omega &= \sum_{k=1}^{N_e} \int_{\Omega_{\mathcal{P}_k}} f(\boldsymbol{x})\, d\Omega, \\
&= \sum_{k=1}^{N_e} \int_{\widetilde{\Omega}_{\mathcal{P}_k}} f(\boldsymbol{x}(\xi,\eta))\left|J^{\xi,\eta}\right|\, d\widetilde{\Omega}, \\
&= \sum_{k=1}^{N_e} \int_{\overline{\Omega}} f(\boldsymbol{x}(\overline{\phi}_{\mathcal{P}_k}(\bar{\xi},\bar{\eta})))\left|J^{\xi,\eta}\right|\left|J^{\bar{\xi},\bar{\eta}}\right|\, d\overline{\Omega}, \\
&= \sum_{k=1}^{N_e} \int_{\overline{\Omega}} f(\bar{\xi},\bar{\eta})\,|J|\, d\overline{\Omega},
\end{aligned} \tag{15}$$

where $N_e$ denotes the total number of patches. It should also be stressed that the integration (15) is also used for the $L^2$-projection procedure used in the isogeometric modified method of characteristics proposed in the present study.

## 3 | ISOGEOMETRIC MODIFIED METHOD OF CHARACTERISTICS

To formulate the Isogeometric modified method of characteristics we first consider the convection part of the problem (1) reformulated for the solution component $u$ using the material derivative as

$$\frac{Du}{Dt} := \frac{\partial u}{\partial t} + \boldsymbol{u} \cdot \nabla u = \boldsymbol{0}, \tag{16}$$

where $\frac{Du}{Dt}$ is the total derivative which measures the rate of change of the solution $u$ following the trajectories of the flow particles. It should be stressed that the main idea of the modified method of characteristics is to impose a regular mesh at the new time level and to backtrack the flow trajectories to the previous time level. The quantities needed at the old time level are approximated by interpolation from their known values on a regular mesh. In what follows we formulate the fundamental steps of the Isogeometric modified method of characteristics proposed in the present study for the solution $u$ and its formulation for the solution component $v$ is carried out in the same manner.

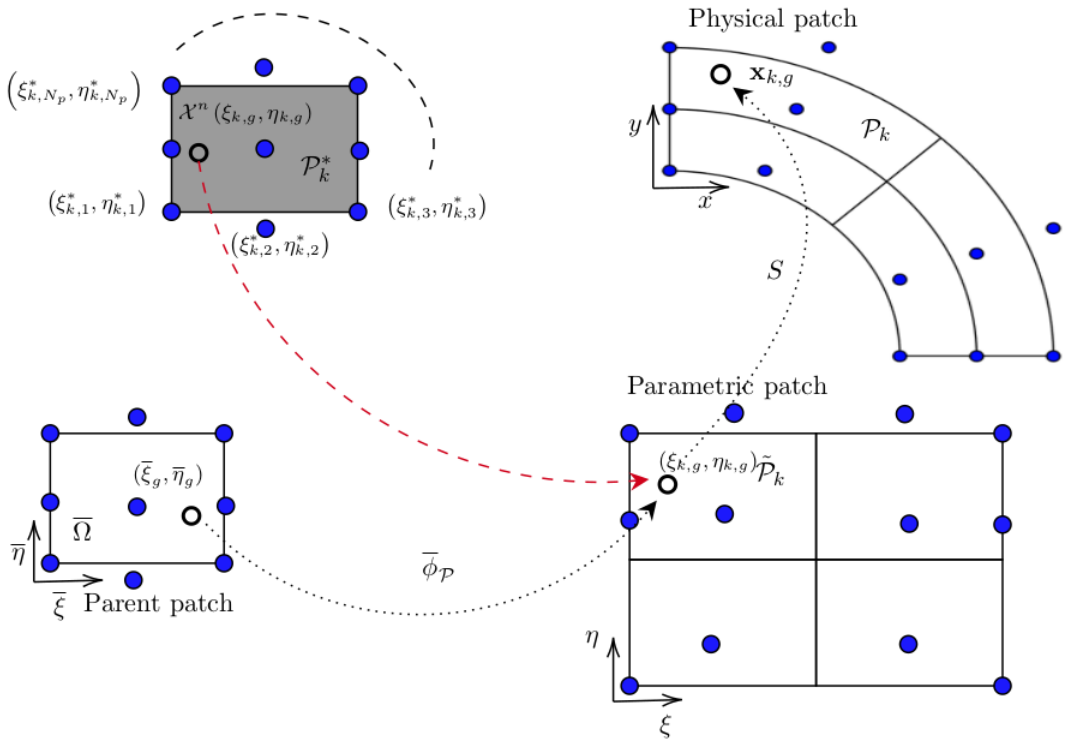


**FIGURE 2** Illustration of the main quantities required for the computation of the departure points. At the first stage, a quadrature point is mapped from the patch $\mathcal{P}_k$ to the patch $\widetilde{\mathcal{P}}_k$. In the second stage, as the NURBS lie in the parametric space, a mapping according to the equation (10), from the parent patch into the parametric patch is required, and results in the departure point $\boldsymbol{\mathcal{X}}^n(\xi_{k,g}, \eta_{k,g})$. Notice that the last transformation is required in order to evaluate the departure points in the parametric space.

## 3.1 | Approximation of departure points

For the space discretization, the computational domain $\Omega$ is partitioned into a set of patches $\mathcal{P}_k$ as $\Omega = \cup_{k=1}^{N_e} \Omega_{\mathcal{P}_k}$, with $N_e$ is the total number of quadrilateral-shaped patches. In the present study, the mesh distribution in the physical space is formed of quadrilaterals constructed by the cross-product of two one-dimensional NURBS functions as illustrated in Figure 2. We also divide the time interval into sub-intervals $[t_n, t_{n+1}]$ with a length $\Delta t$. Note that in general, since the control points do not lie on the physical geometry, the NURBS polynomials are not interpolatory, see for instance[28]. In the present study, to overcome this drawback in the NURBS we consider the $L^2$-projection approach introduced in[22]. Thus, for each patch $\mathcal{P}_k$ in the computational domain $\Omega$ we consider its associated quadrature points $\boldsymbol{x}_{k,g} = \left(x_{k,g}, y_{k,g}\right)^\top$ with the corresponding weights $\omega_{k,g}$ for $g = 1, \ldots, N_{k,g}$ with $N_{k,g}$ is the total number of quadrature points in the patch $\mathcal{P}_k$. Hence, the characteristic curves $\boldsymbol{\mathcal{X}}(\tau, \boldsymbol{x}_{k,g})$ associated with the convection problem (1) are calculated for each quadrature point $\boldsymbol{x}_{k,g}$ by solving the backward differential equations

$$\begin{aligned} \frac{d\boldsymbol{\mathcal{X}}(\tau, \boldsymbol{x}_{k,g})}{d\tau} &= \boldsymbol{u}(\boldsymbol{\mathcal{X}}(\tau, \boldsymbol{x}_{k,g})), \qquad \forall\, \tau \in [t_n, t_{n+1}], \\ \boldsymbol{\mathcal{X}}(t_{n+1}, \boldsymbol{x}_{k,g}) &= \boldsymbol{x}_{k,g}, \end{aligned} \tag{17}$$

where $\boldsymbol{\mathcal{X}}(\tau, \boldsymbol{x}_{k,g}) = \left(X(\tau, \boldsymbol{x}_{k,g}), Y(\tau, \boldsymbol{x}_{k,g})\right)^\top$ is the departure point defined at time $\tau$ of a particle that will reach $\boldsymbol{x}_{k,g} = \left(x_{k,g}, y_{k,g}\right)^\top$ at time $t_{n+1}$. It should be noted that the modified method of characteristics does not follow the flow particles forward in time as a Lagrangian method does, instead it traces backwards the position at time $t_n$ of particles that will reach the points of a fixed mesh at time $t_{n+1}$, see Figure 2 for an illustration. Therefore, the modified method of characteristics avoids the grid distortion difficulties that the conventional Lagrangian schemes have. It should be stressed that, in a purely Lagrangian approach, the mesh is expected to be distorted to a degree that invalidates computational results and it necessitates remeshing in order to

update the solution at the next time level. However, remeshing is computationally very demanding and can often lead to inaccuracies in the computed solutions that are projected onto a new mesh[29]. It is also well known that, in the purely Lagrangian schemes, the fluid particles are followed forward in time. Thus, the computational mesh should be deformed at every time step in order to adapt it to a new configuration. This is not the case for the proposed modified method of characteristics (also known in the literature by semi-Lagrangian methods) as the particles are followed in a backward manner according to the initial-value problem (17). Hence, the mesh remains fixed and do not move during the time evolution and this is one of the main advantages of semi-Lagrangian methods compared to its purely Lagrangian counterparts.

Note that accurate approximations of the characteristic curves $\boldsymbol{\mathcal{X}}(\tau, \boldsymbol{x}_{k,g})$ are crucial to the overall accuracy of the modified method of characteristics. In[22,23], a second-order extrapolation based on the mid-point rule is used to approximate the solution of (17), but this method involves an iterative procedure which may become computationally demanding. In the current work, we consider the third-order explicit Runge-Kutta method proposed in[30]. Thus, the procedure to approximate the solution of the differential equations (17) can be achieved by

$$\begin{aligned} \mathbf{K}_{k,g}^{(1)} &= \boldsymbol{x}_{k,g} - \Delta t \boldsymbol{u}^n \left(\boldsymbol{x}_{k,g}\right), \\ \mathbf{K}_{k,g}^{(2)} &= \frac{3}{4}\boldsymbol{x}_{k,g} + \frac{1}{4}\mathbf{K}_{k,g}^{(1)} - \frac{1}{4}\Delta t \boldsymbol{u}^n \left(\mathbf{K}_{k,g}^{(1)}\right), \\ \boldsymbol{\mathcal{X}}(t_n, \boldsymbol{x}_{k,g}) &= \frac{1}{3}\boldsymbol{x}_{k,g} + \frac{2}{3}\mathbf{K}_{k,g}^{(2)} - \frac{2}{3}\Delta t \boldsymbol{u}^n \left(\mathbf{K}_{k,g}^{(2)}\right). \end{aligned} \tag{18}$$

In general the departure points $\boldsymbol{\mathcal{X}}(t_n, \boldsymbol{x}_{k,g})$ do not coincide with the spatial position of the point $\boldsymbol{x}_{k,g}$. To find the host element where such point is located we adapt the search-locate algorithm proposed in[31] for quadrilateral elements. Note that the NURBS do not provide a direct way to compute the coordinates in the parametric space given its physical space location and therefore a nonlinear equation is needed to be solved using the Gauss-Newton method, see[32] among others. Hence, integrating the convection equation (16) along the characteristic curves yields

$$u^{n+1}(\boldsymbol{x}) = u^n \circ \boldsymbol{\mathcal{X}}^n(\boldsymbol{x}), \tag{19}$$

where $\boldsymbol{\mathcal{X}}^n(\boldsymbol{x}) = \boldsymbol{\mathcal{X}}(t_n, \boldsymbol{x})$ is a notation to emphasis the dependence of the departure points $\boldsymbol{\mathcal{X}}$ on the mesh point $\boldsymbol{x}$. In the current study, the solution at the next time level is obtained by a weak formulation using the $L^2$-projection. Thus, multiplying both sides of (19) by the NURBS function $R_m^{p,q}$ and integrating the resulting equation over $\Omega$, it leads to the following weak form

$$\int_\Omega u^{n+1}(\boldsymbol{x}) R_m^{p,q}(\boldsymbol{x})\, d\Omega = \int_\Omega u^n(\boldsymbol{\mathcal{X}}^n) R_m^{p,q}(\boldsymbol{x})\, d\Omega, \qquad m = 1, \ldots, \mathrm{DoF}. \tag{20}$$

Thus, the isogeometric finite element solution $u^{n+1}(\boldsymbol{x})$ can be formulated as

$$u^{n+1}(\boldsymbol{x}) = \sum_{l=1}^{\mathrm{DoF}} U_l^{n+1} R_l^{p,q}(\boldsymbol{x}), \tag{21}$$

where $U_l^{n+1}$ are the unknown nodal coefficients of the solution. Next, replacing (21) in the left-hand side of (20) we obtain

$$\begin{aligned} \int_\Omega u^{n+1}(\boldsymbol{x}) R_m^{p,q}(\boldsymbol{x})\, d\Omega &= \int_\Omega \sum_{l=1}^{\mathrm{DoF}} U_l^{n+1} R_l^{p,q}(\boldsymbol{x}) R_m^{p,q}(\boldsymbol{x})\, d\Omega, \\ &= \sum_{l=1}^{\mathrm{DoF}} U_l^{n+1} \int_\Omega R_l^{p,q}(\boldsymbol{x}) R_m^{p,q}(\boldsymbol{x})\, d\Omega, \\ &:= \sum_{l=1}^{\mathrm{DoF}} a_{ml} U_l^{n+1}, \end{aligned} \tag{22}$$

with $a_{ml} = \int_\Omega R_l^{p,q}(\boldsymbol{x}) R_m^{p,q}(\boldsymbol{x})\, d\Omega$. The crucial idea behind the $L^2$-projection approach is the computation of the right-hand integral in (20). In a general framework, it is challenging to evaluate this integral exactly and one has to use the quadrature rules. Numerical integration is one of the most issues affecting the efficiency and accuracy in Galerkin-based finite element methods. In addition to the isogeometric paradigm of assembling systems of equations which requires the calculation of integrals in the mass and stiffness matrices, the $L^2$-projection approach necessitates the calculation of integrals in the right-hand side of (20). For this purpose, Gauss-based quadrature rules have extensively been used to approximate these integrals for quadrilateral and tetrahedral elements, see for example[33]. In[34] a class of optimal Gauss-based quadrature rules (Gauss-Radau rule) has been

developed for spline spaces which usually occur in Galerkin-based finite element discretizations for which the original spaces are $\mathcal{C}^1$ quadratics or $\mathcal{C}^2$ cubics. In the current work, we adopt the Gauss-Jacobi quadrature rule used also in [35,36,37,38] among others. It should also be noted that the Gauss-based quadrature rules are known to exhibit fast convergence, and the full tensor product Gauss-Jacobi quadrature rule is proven to converge exponentially and it is exact for polynomials of degree up to $2m-1$, see for instance [36]. Hence, using Gauss-Jacobi quadrature rule, the integral in right-hand side of (20) is evaluated as

$$\begin{aligned}
\int_{\Omega} u^n(\boldsymbol{\mathcal{X}}^n) R_m^{p,q}(\boldsymbol{x})\, d\Omega &= \sum_{k=1}^{N_e} \int_{\Omega_{\mathcal{P}_k}} u^n \circ \boldsymbol{\mathcal{X}}^n(\boldsymbol{x}) R_m^{p,q}(\boldsymbol{x})\, d\Omega, \\
&= \sum_{k=1}^{N_e} \int_{\bar{\Omega}} u^n \circ \boldsymbol{\mathcal{X}}^n(\bar{\xi},\bar{\eta}) R_m^{p,q}(\bar{\xi},\bar{\eta}) \left|J(\bar{\xi},\bar{\eta})\right|\, d\bar{\Omega}, \\
&\approx \sum_{k=1}^{N_e} \sum_{g=1}^{N_{k,g}} w_{k,g} u^n \circ \boldsymbol{\mathcal{X}}^n(\bar{\xi}_g,\bar{\eta}_g) R_m^{p,q}(\bar{\xi}_g,\bar{\eta}_g) \left|J(\bar{\xi}_g,\bar{\eta}_g)\right|, \\
&\approx \sum_{k=1}^{N_e} \sum_{g=1}^{N_{k,g}} w_{k,g} \widetilde{u}_{k,g}^n R_m^{p,q}(\bar{\xi}_g,\bar{\eta}_g) \left|J(\bar{\xi}_g,\bar{\eta}_g)\right| := r_m^n, \qquad m = 1,\dots,\mathrm{DoF},
\end{aligned} \tag{23}$$

where $\widetilde{u}_{k,g}^n = u^n(\boldsymbol{\mathcal{X}}^n(\boldsymbol{x}_{k,g}))$ denotes the solution calculated at the departure point $\boldsymbol{\mathcal{X}}^n(\boldsymbol{x}_{k,g})$. Here, the values $\widetilde{u}_{k,g}^n$ are computed as

$$\widetilde{u}_{k,g}^n := u^n(\boldsymbol{\mathcal{X}}^n(\boldsymbol{x}_{k,g})) = \sum_{d=1}^{N_p} u^n(\xi_{k,d}^*, \eta_{k,d}^*) R_d^{p,q}(\boldsymbol{\mathcal{X}}^n(\boldsymbol{x}_{k,g})), \tag{24}$$

where $u^n(\xi_{k,d}^*, \eta_{k,d}^*)$ are the known solutions at the control points $(\xi_{k,d}^*, \eta_{k,d}^*)$ of the host patch $\mathcal{P}_k^*$ where the departure point $\boldsymbol{\mathcal{X}}^n(\boldsymbol{x}_{k,g})$ belongs. Here, $N_p$ is the total number of control points affecting the host patch $\mathcal{P}_k^*$ which is immediately related to the order of NURBS basis functions, see Figure 2 for an illustration. Thus, injecting the approximations (22) and (23) in (20) yields

$$\sum_{l=1}^{\mathrm{DoF}} a_{ml} U_l^{n+1} = r_m^n, \qquad m = 1,\dots,\mathrm{DoF}, \tag{25}$$

where

$$r_m^n = \sum_{k=1}^{N_e} \sum_{g=1}^{N_{k,g}} w_{k,g} \widetilde{u}_{k,g}^n R_m^{p,q}(\bar{\xi}_g,\bar{\eta}_g) \left|J(\bar{\xi}_g,\bar{\eta}_g)\right|, \tag{26}$$

and

$$\begin{aligned}
a_{ml} &= \int_{\Omega} R_l^{p,q}(\boldsymbol{x}) R_m^{p,q}(\boldsymbol{x})\, d\Omega, \\
&= \sum_{k=1}^{N_e} \int_{\Omega_{\mathcal{P}_k}} R_l^{p,q}(\boldsymbol{x}) R_m^{p,q}(\boldsymbol{x})\, d\Omega_{\mathcal{P}_k}, \\
&= \sum_{k=1}^{N_e} \int_{\bar{\Omega}} R_l^{p,q}(\bar{\xi},\bar{\eta}) R_m^{p,q}(\bar{\xi},\bar{\eta}) \left|J(\bar{\xi},\bar{\eta})\right|\, d\bar{\Omega}, \\
&\approx \sum_{k=1}^{N_e} \sum_{g=1}^{N_{k,g}} w_{k,g} R_l^{p,q}(\bar{\xi}_g,\bar{\eta}_g) R_m^{p,q}(\bar{\xi}_g,\bar{\eta}_g) \left|J(\bar{\xi}_g,\bar{\eta}_g)\right|.
\end{aligned} \tag{27}$$

Note that the equation (25) can also be assembled in a global matrix-vector form as

$$[\mathbf{M}] \left\{\boldsymbol{U}^{n+1}\right\} = \{\mathbf{r}^n\}, \tag{28}$$

where $[\mathbf{M}]$ is the DoF$\times$DoF-valued isogeometric $L^2$-projection mass matrix with entries $a_{ml}$, $\left\{\boldsymbol{U}^{n+1}\right\}$ is the DoF-valued vector of unknown nodal values of the solution $U_m^{n+1}$ at time $t_{n+1}$, and $\{\mathbf{r}^n\}$ is the DoF-valued vector of the known right-hand side with entries $r_m^n$. Notice that the integrals $a_{ml}$ and the components $r_m^n$ of the right-hand side in equations (26) and (27) can be evaluated using the Gauss-Jacobi quadrature rule as explained in (15). In summary, the Isogeometric modified method of characteristics to solve the convection problem (16) is carried out in the steps described in Algorithm 1. These same steps are also performed

to compute solution component $v^{n+1}$ in the convection part (16) of the Burgers' system. For convenience of the reader, the Gauss-Jacobi quadrature rule used in our Isogeometric modified method of characteristics is provided in the appendix.

**Algorithm 1** Algorithm for the Isogeometric modified method of characteristics.

1: Compute $a_{ml}$ using (27) and assemble the $L^2$-projection mass matrix [**M**].
2: Assuming the nodal solution $\mathbf{U}^n$ is known.
3: **for** For each patch $\mathcal{P}_k$ $(k = 1 \dots, N_e)$ in the computational mesh **do**
4: Generate the quadrature points and corresponding weights $\left(\boldsymbol{x}_{k,g}, w_{k,g}\right)$ $(g = 1, \dots, N_g)$.
5: **for** For each quadrature point $\boldsymbol{x}_{k,g}$, $g = 1, \dots, N_g$ **do**
6: Compute the departure point $\boldsymbol{\mathcal{X}}^n(\boldsymbol{x}_{k,g})$ by solving the initial-value problem (17).
7: Identify the host patch $\mathcal{P}_k^*$ where the departure point $\boldsymbol{\mathcal{X}}^n(\boldsymbol{x}_{k,g})$ belongs.
8: Compute the parametric coordinates $\boldsymbol{\mathcal{X}}^n(\xi_{k,g}, \eta_{k,g})$ associated with the parent coordinates $\boldsymbol{\mathcal{X}}^n(\boldsymbol{x}_{k,g})$ using (10).
9: Evaluate the NURBS functions $R(\boldsymbol{\mathcal{X}}^n(\xi_{k,g}, \eta_{k,g}))$ using the tensor product of (5).
10: Calculate the solution value $\widetilde{u}_{k,g}$ using the approximation (24).
11: **end for**
12: Compute the elements $r_m^n$ using (26) and assemble the right hand-side vector $\{\mathbf{r}^n\}$.
13: **end for**
14: Solve the linear system (28) to obtain the solution $\left\{\mathbf{U}^{n+1}\right\}$.
15: Calculate the solution component $u^{n+1}$ at time $t_{n+1}$ using (21).

## 3.2 | Solution of the diffusion part

In the current study, to solve the diffusive part in the Burgers' equations (1) we consider the explicit third-order Runge-Kutta method along the characteristics. Thus, assuming the convection part in (1) is dealt with using the modified method of characteristic as described above, then the weak formulation reads as follows: Find $\left(u_h, v_h\right) \in \mathcal{W}_h \times \mathcal{W}_h$ such that

$$\int_\Omega \frac{Du_h}{Dt}\phi_h \, d\Omega + \frac{1}{Re}\int_\Omega \nabla u_h \cdot \nabla \phi_h \, d\Omega = 0, \qquad \forall\, \phi_h \in \mathcal{W}_h, \tag{29a}$$

$$\int_\Omega \frac{Dv_h}{Dt}\phi_h \, d\Omega + \frac{1}{Re}\int_\Omega \nabla v_h \cdot \nabla \phi_h \, d\Omega = 0, \qquad \forall\, \phi_h \in \mathcal{W}_h, \tag{29b}$$

where $\mathcal{W}_h$ is the conforming finite element space. Note that an advantage of the modified method of characteristics lies on the fact that the equations (29a)-(29b) are decoupled and can be solved separately for each solution component. Therefore, for brevity in the presentation, the method is formulated only for the component $u$ and the same procedure is carried out for the component $v$. Hence, the approximation of the solution $u$ is written in terms of the NURBS basis functions as

$$u_h(\boldsymbol{x}) = \sum_{l=1}^{\text{DoF}} U_l R_l^{p,q}(\boldsymbol{x}), \tag{30}$$

where $\{U_l\}$ represents the set of all unknown control variables. Likewise, the test function is discretized as

$$w_h(\boldsymbol{x}) = \sum_{m=1}^{\text{DoF}} W_m R_m^{p,q}(\boldsymbol{x}). \tag{31}$$

Substituting the equations (31) and (30) into (29a), the semi-discrete form is now written as

$$\frac{D}{Dt}\left(\sum_{m=1}^{\text{DoF}}\sum_{l=1}^{\text{DoF}}\int_\Omega R_l^{p,q} R_m^{p,q} \, d\Omega\right) U_l + \frac{1}{Re}\left(\sum_{m=1}^{\text{DoF}}\sum_{l=1}^{\text{DoF}}\int_\Omega \nabla R_l^{p,q} \cdot \nabla R_m^{p,q} \, d\Omega\right) U_l = 0, \tag{32}$$

for $l = 1, \ldots, \text{DoF}$. In a matrix compact form, the semi-discrete form (32) can be expressed as

$$[\mathbf{M}]\,\frac{D\mathbf{U}}{Dt} + \frac{1}{Re}\,[\mathbf{S}]\,\mathbf{U} = \mathbf{0}, \tag{33}$$

with a similar system for the solution component $v$. Here, $\mathbf{U} = \left(U_1, \ldots, U_{\text{DoF}}\right)^T$, $[\mathbf{M}]$ and $[\mathbf{S}]$ are the well-known mass and stiffness matrices the elements of which are given by

$$a_{ml} = \int_{\Omega} R_l^{p,q} R_m^{p,q}\, d\Omega, \qquad m, l = 1, 2 \ldots, \text{DoF},$$

and

$$\mathcal{S}_{ml} = \int_{\Omega} \nabla R_l^{p,q} \cdot \nabla R_m^{p,q}\, d\Omega, \qquad m, l = 1, 2 \ldots, \text{DoF},$$

respectively. Note that the assembly of matrices $[\mathbf{M}]$ and $[\mathbf{S}]$ is performed using the parent coordinate system along with the mappings from the physical space to the parametric space to the parent space and its associated Jacobian matrices. The time integration of the system (33) is complete once a time-stepping scheme is chosen for the numerical solution. In the present work, we solve the system (33) using the third-order explicit Runge-Kutta method as

$$\begin{aligned}
\mathcal{U}^{(1)} &= \widetilde{\mathbf{U}}^n + \Delta t \mathbf{F}\left(\widetilde{\mathbf{U}}^n\right), \\
\mathcal{U}^{(2)} &= \frac{3}{4}\widetilde{\mathbf{U}}^n + \frac{1}{4}\mathcal{U}^{(1)} + \frac{1}{4}\Delta t \mathbf{F}\left(\mathcal{U}^{(1)}\right), \\
\mathbf{U}^{n+1} &= \frac{1}{3}\widetilde{\mathbf{U}}^n + \frac{2}{3}\mathcal{U}^{(2)} + \frac{2}{3}\Delta t \mathbf{F}\left(\mathcal{U}^{(2)}\right),
\end{aligned} \tag{34}$$

where $\mathbf{F}(\mathbf{U})$ is the right-hand-side function associated with (33) as

$$\mathbf{F}(\mathbf{U}) = \frac{1}{Re}\,[\mathbf{M}]^{-1}\,[\mathbf{S}]\,\mathbf{U},$$

and $\widetilde{\mathbf{U}}^n$ is solution vector with entries $\widetilde{u}_{k,g}^n$ computed in (24). Note that the main advantage of this scheme lies on the fact that (34) is a convex combination of the first-order Euler steps which exhibits strong stability properties. Therefore, the scheme (34) is TVD, third-order accurate in time, and stable under the conventional Courant-Friedrichs-Lewy (CFL) condition. It should be noted that the inverse of the matrix $[\mathbf{M}]$ in (33) is required to be computed and stored once during the time-stepping procedure. Here, the system matrix may be decomposed at the first time step and retained to be reused with just updating the right-hand side of the linear system of equations at all the following time steps.

## 4 | NUMERICAL RESULTS

In this section we assess the numerical performance of the new isogeometric modified method of characteristics using three examples in different computational domains. For these test examples, the analytical solutions are known, so that we can evaluate the relative $L^1$-error and $L^2$-error at time $t_n$ as

$$L^1\text{-error} = \frac{\displaystyle\int_{\Omega} \left|u_h^n - u_{\text{exact}}(\boldsymbol{x}_h, t_n)\right| d\boldsymbol{x}}{\displaystyle\int_{\Omega} \left|u_{\text{exact}}^n(\boldsymbol{x}_h, t_n)\right| d\boldsymbol{x}}, \qquad L^2\text{-error} = \frac{\displaystyle\left(\int_{\Omega} \left|u_h^n - u_{\text{exact}}^n(\boldsymbol{x}_h, t_n)\right|^2 d\boldsymbol{x}\right)^{\frac{1}{2}}}{\displaystyle\left(\int_{\Omega} \left|u_{\text{exact}}^n(\boldsymbol{x}_h, t_n)\right|^2 d\boldsymbol{x}\right)^{\frac{1}{2}}}, \tag{35}$$

where $u_{\text{exact}}(\boldsymbol{x}_h, t_n)$ and $u_h^n$ are respectively, the exact and numerical solutions at time $t_n$ in the mesh point $\boldsymbol{x}_h$. We also define the CFL number associated with the equations (1) as

$$\text{CFL} = \max\left(\max_{\boldsymbol{x}} \sqrt{|u^n|^2 + |v^n|^2}\,\frac{\Delta t_n}{h}, \frac{\Delta t_n}{Re h^{p+1}}\right). \tag{36}$$

Note that the last term in the condition (36) accounts for the explicit treatment of the diffusion part in the Burgers equations by the explicit Runge-Kutta scheme (18). In all results reported in this section, the CFL number is fixed to CFL = 3 and a variable time

step $\Delta t_n$ is used in the simulations according to the condition (36). It should be stressed that the CFL number in (36) accounts for both the convection and diffusion parts in the problem (1). Similar estimates have been derived in [39] for convection-diffusion equations. All our computations were performed on an Intel^ Core(TM) i7-7500U @ 2.70GHz with 16 GB of RAM.

## 4.1 | Example 1

We solve the coupled Burgers' equations (1) in a squared domain $\Omega = [-2, 2] \times [-2, 2]$ with initial and Dirichlet boundary conditions obtained from the following analytical solution

$$\begin{aligned} u(x, y, t) &= \frac{1}{2}\left(1 - \tanh\left(\frac{Re}{4}(x + y - t)\right)\right), \\ v(x, y, t) &= \frac{1}{2}\left(1 - \tanh\left(\frac{Re}{4}(x + y - t)\right)\right). \end{aligned} \tag{37}$$

This example has been widely used in the literature to examine numerical methods for solving the two-dimensional Burgers' equations, see for instance [18,19,20,21]. Here, the exact solution (37) is used to quantify the errors in the proposed isogeometric modified method of characteristics for solving the Burgers' system for three different Reynolds numbers $Re = 10^1$, $Re = 10^4$ and $Re = 10^8$ at time $t = 1$ using different NURBS degrees. In all our simulations, a uniform mesh consisting of 32×32 grids of square patches with patch side length $h = 1/32$ is considered. Refinements are performed by the $k$-refinement method, and the numerical solutions are computed using different degrees ranging from $p = 1$ to $p = 5$. In all cases, we omit the results for the component $v$ and we present the numerical solution of the component $u$ only for brevity in the presentation.

In Figure 3 we present the solution $u$ obtained using NURBS of orders $p = 2$, 3 and 4 at time $t = 1$ using a uniform mesh with $32 \times 32$ elements. For comparison reasons, analytical solutions are also presented in this figure. The clear indication from these results is that at Reynolds numbers $Re = 10$ and $Re = 10^4$, no significant differences between the results obtained using the selected polynomial orders. However, at Reynolds number $Re = 10^8$, the results obtained using the quadratic and cubic polynomials exhibit oscillations at the shock areas where large gradients appear. On the other hand, the solution obtained using the quartic polynomial is in good agreement with the exact solution for this case with $Re = 10^8$. Note that at high Reynolds numbers, the convection terms in the Burgers system (1) become highly dominant for which non-physical oscillations are expected when using high polynomial orders in the discretization, see for example [1,40]. This is not the case in the proposed isogeometric modified method of characteristics mainly because (i) the modified method of characteristics is proven to be unconditionally stable, see for instance [41,42,43], and (ii) the potential of the $k$-refinement strategy in offering high inter-element continuity by providing smoother functions than the conventional finite element methods, see [24,25,44] among others. The corresponding cross-sections at the main diagonal $y = 1 - x$ of the solution $u$ are displayed in Figure 4 using linear, quadratic, cubic and quartic NURBS polynomials. As expected, solutions obtained using linear NURBS polynomials exhibits large numerical dissipation near the shock areas for $Re = 10$ and $Re = 10^4$ whereas, solutions obtained using cubic and quartic NURBS polynomials show a good behavior compared to the exact solution. Again for $Re = 10^8$, solutions obtained using $p = 1$, 2 and 3 exhibit non-physical oscillations at zones with sharp gradients and fail to preserve the monotonicity of the computed solutions, compare the overshots and undershoots in the results shown in Figure 4. However, increasing the NURBS degree to $p = 4$, the non-physical oscillations in the computed solutions disappear and the shock is very well captured. The resolution of the proposed isogeometric modified method of characteristics is highly observed for this example and no oscillations have been detected in the vicinity of steep gradients.

To study the convergence behavior of the proposed isogeometric modified method of characteristics, we report in Table 1 the $L^1$-error and the corresponding convergence rates using different NURBS orders and different Reynolds numbers. It is clear that, maintaining the NURBS order fixed and adopting the $h$-refinement yields a decay of all computed errors. For instance, at the low Reynolds number $Re = 10$ for which the diffusion is relatively dominated, obtaining satisfactory results is evident in this situation and we believe that the $p$-refinement strategy is precise enough in this case. Indeed, the optimal convergence rates are captured for all NURBS orders at the considered Reynolds numbers. At the moderate Reynolds number $Re = 10^4$ which can be considered as a critical value for which shocks are observed in the computed solutions, it can be noticed from Table 1 that all optimal orders are still achieved. At the high Reynolds number $Re = 10^6$ corresponding to strong shock and thus less accuracy is observed in the shock zones in the computed solutions. Consequently, the accuracy of the numerical results is reduced for such values of Reynolds numbers. This can immediately be observed in the reduction of convergence rates for $Re = 10^6$. Similar features have also been observed in the results, not reported here for brevity, obtained using the $L^2$-error.

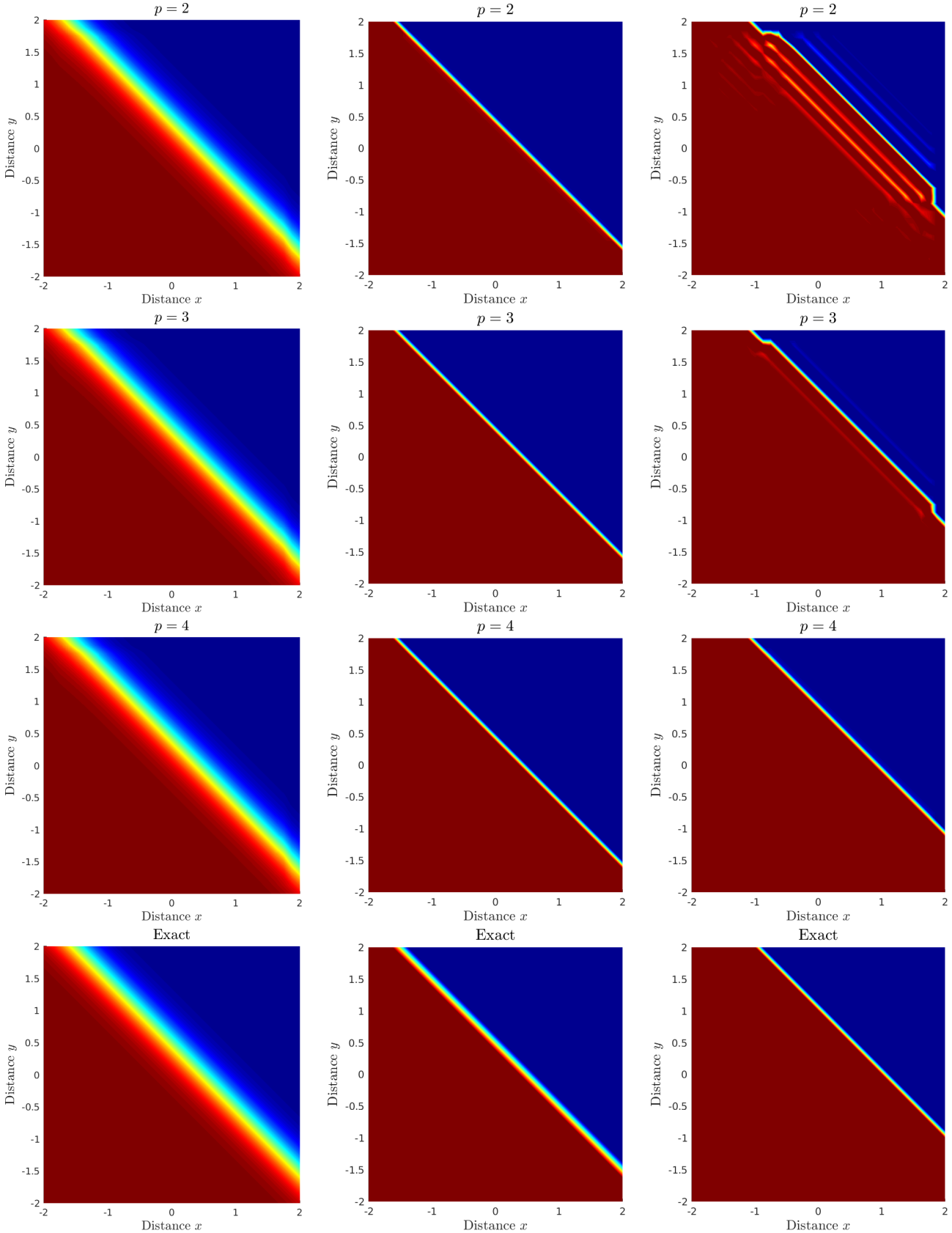


**FIGURE 3** Results for the solution $u$ in Example 1 at time $t = 1$ obtained using a mesh of $32 \times 32$ elements with $p = 2$ (first row), $p = 3$ (second row), $p = 4$ (third row) and the exact solution (fourth row). Here, $Re = 10$ (first column), $Re = 10^4$ (second column) and $Re = 10^8$ (third column).

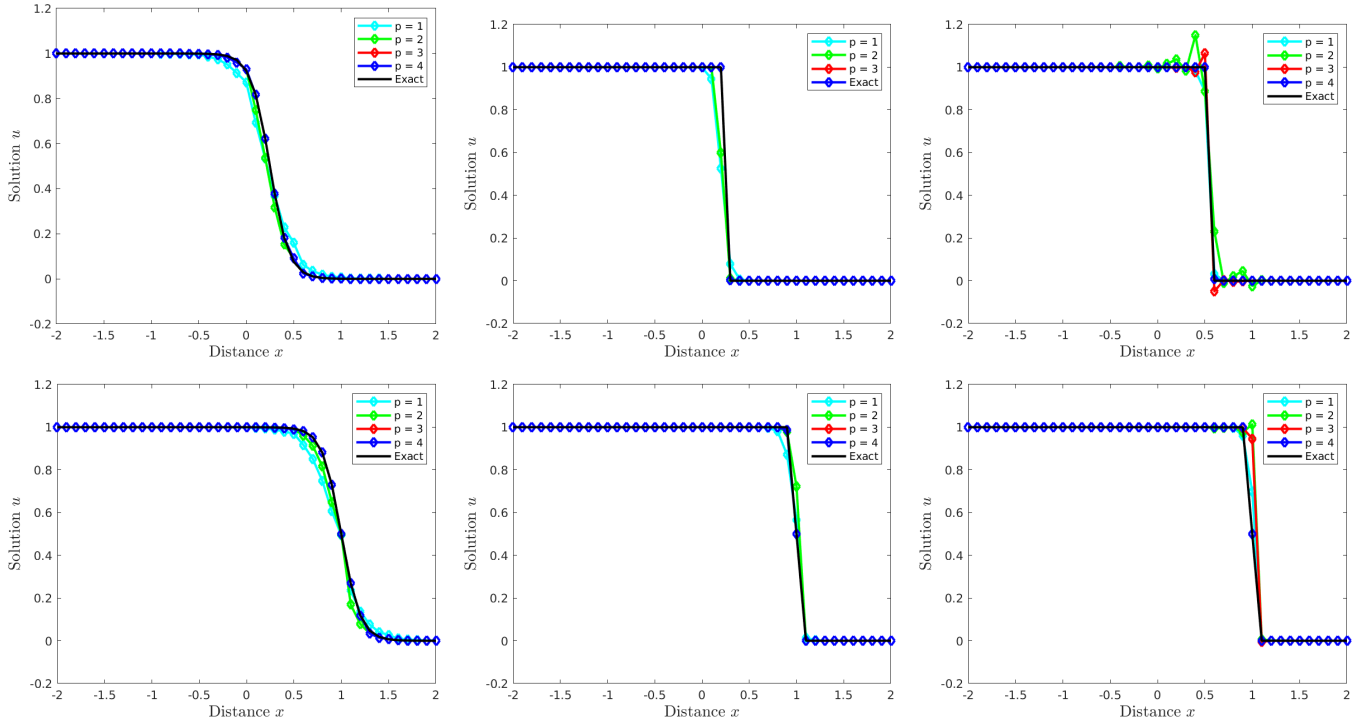


**FIGURE 4** Cross-sections at the diagonal $y = 1 - x$ of the solution $u$ obtained for Example 1 at time $t = 1$ (top) and $t = 2$ (bottom) on a mesh of $32 \times 32$ elements using different NURBS degrees for $Re = 10$ (left plot), $Re = 10^4$ (middle plot) and $Re = 10^8$ (right plot).

## 4.2 | Example 2

In this example we solve the coupled Burgers' equations (1) in the squared domain $\Omega = [0, 1] \times [0, 1]$ with initial and Dirichlet boundary conditions obtained from the following analytical solution

$$\begin{aligned} u(x, y, t) &= \frac{3}{4} - \frac{1}{4\left(1 + \exp\left(-\frac{(4x - 4y + t)Re}{32}\right)\right)}, \\ v(x, y, t) &= \frac{3}{4} + \frac{1}{4\left(1 + \exp\left(-\frac{(4x - 4y + t)Re}{32}\right)\right)}. \end{aligned} \tag{38}$$

The exact solution (38) is used to quantify the errors in the proposed isogeometric modified method of characteristics for solving the Burgers' equations for four different Reynolds numbers $Re = 10^2$, $10^3$, $10^4$ and $10^5$ at time $t = 1$ using different NURBS degrees. In all our calculations, the mesh is uniform consisting of a 32×32 mesh of squared patches, with patch side length $h = 1/32$. Refinements are also performed by the $k$-method and numerical results are presented for different degrees $p$. Again for brevity, we omit the results for the component $v$ and we present the numerical results for the component $u$ only. In Table 2 we summarize the relative $L^1$-error, relative $L^2$-error and convergence rates for the proposed isogeometric modified method of characteristics using $Re = 10^2$ and $Re = 10^3$. Those results obtained using $Re = 10^4$ and $Re = 10^5$ are presented in Table 3. It is clear that refining the mesh or NURBS degree results in a decrease in the relative $L^1$-error and $L^2$-error for all considered Reynolds numbers. In addition, better convergence rates are obtained for all considered meshes for the simulations using low Reynolds numbers ($Re = 10^2$ and $Re = 10^3$) than using high Reynolds numbers ($Re = 10^4$ and $Re = 10^5$). Moreover, the optimal convergence rates are achieved after some saturation for the selected NURBS degrees. It is also evident from the results reported in Table 2 and Table 3 that the convergence rates in the proposed isogeometric modified method of characteristics are not highly affected by the Reynolds numbers taken in the simulations. Therefore, fixing the NURBS degree and adopting $h$-refinement results in a decrease of all errors for the considered Reynolds numbers. It also is evident that the new

**TABLE 1** Results for Example 1 obtained using different meshes and NURBS degrees for three different Reynolds numbers at time $t = 1$.

| | | $Re = 10$ | | $Re = 10^4$ | | $Re = 10^6$ | |
|---|---|---|---|---|---|---|---|
| $p$ | # patches | $L^1$-error | Rate | $L^1$-error | Rate | $L^1$-error | Rate |
| 1 | 2×2 | 2.99585E-01 | — | 5.79140E-01 | — | 5.86201E-01 | — |
| | 4×4 | 1.39068E-01 | 1.1072 | 4.18147E-01 | 0.4699 | 4.22094E-01 | 0.4738 |
| | 8×8 | 6.44202E-02 | 1.1102 | 3.76509E-01 | 0.1513 | 3.79003E-01 | 0.1554 |
| | 16×16 | 3.00010E-02 | 1.1025 | 1.79402E-01 | 1.0695 | 1.84012E-01 | 1.0424 |
| | 32×32 | 1.37400E-02 | 1.1266 | 9.42409E-02 | 0.9288 | 9.49514E-02 | 0.9545 |
| 2 | 2×2 | 2.50535E-01 | — | 5.22051E-01 | — | 5.30112E-01 | — |
| | 4×4 | 1.01068E-01 | 1.3097 | 3.25530E-01 | 0.6814 | 3.29814E-01 | 0.6846 |
| | 8×8 | 2.51202E-02 | 2.0084 | 1.27176E-01 | 1.3560 | 1.34270E-01 | 1.2965 |
| | 16×16 | 6.08010E-03 | 2.0467 | 5.61230E-02 | 1.1802 | 5.70114E-02 | 1.2358 |
| | 32×32 | 1.46750E-03 | 2.0507 | 9.94120E-03 | 2.4971 | 9.98347E-03 | 2.5136 |
| 3 | 2×2 | 4.07337E-02 | — | 8.12345E-02 | — | 8.20766E-02 | — |
| | 4×4 | 1.30294E-02 | 1.6445 | 2.76539E-02 | 1.5546 | 2.80322E-02 | 1.5499 |
| | 8×8 | 2.94538E-03 | 2.1452 | 5.34985E-03 | 2.3699 | 5.41033E-03 | 2.3733 |
| | 16×16 | 2.55297E-04 | 3.5282 | 5.13475E-04 | 3.3811 | 5.22512E-04 | 3.3722 |
| | 32×32 | 2.10699E-05 | 3.5989 | 4.14879E-05 | 3.6295 | 5.22118E-05 | 3.3230 |
| 4 | 2×2 | 2.78277E-02 | — | 5.26985E-02 | — | 5.32778E-02 | — |
| | 4×4 | 5.02555E-03 | 2.4692 | 1.02598E-02 | 2.3608 | 1.13432E-02 | 2.2317 |
| | 8×8 | 3.04425E-04 | 4.0451 | 6.11340E-04 | 4.0689 | 6.91287E-04 | 4.0364 |
| | 16×16 | 1.80312E-05 | 4.0775 | 3.35463E-05 | 4.1877 | 3.90877E-05 | 4.1445 |
| | 32×32 | 1.05456E-06 | 4.0958 | 2.23482E-06 | 3.9079 | 2.39910E-06 | 4.0261 |
| 5 | 2×2 | 2.50257E-03 | — | 5.03415E-03 | — | 5.41230E-03 | — |
| | 4×4 | 3.03302E-04 | 3.0446 | 6.16575E-04 | 3.0294 | 6.70621E-04 | 3.0127 |
| | 8×8 | 1.77803E-05 | 4.0924 | 3.24607E-05 | 4.2475 | 3.49711E-05 | 4.2613 |
| | 16×16 | 5.82775E-07 | 4.9312 | 1.71385E-06 | 4.2434 | 2.00211E-06 | 4.1266 |
| | 32×32 | 1.78082E-08 | 5.0323 | 3.28485E-08 | 5.7053 | 6.01744E-08 | 5.0562 |

isogeometric modified method of characteristics shows an accuracy of the expected orders. Notice that, coarse meshes are used in our simulations to illustrate the $p$-convergence of the proposed isogeometric modified method of characteristics for solving the Burgers' equations. Using finer meshes than those used in Table 2 and Table 3 would not improve the achieved convergence rates.

Next we examine the performance of the proposed isogeometric modified method of characteristics for solving the Burgers' equations in complex domains. To this end, we solve the equations (1) in a unit circular domain centered at $(0.5, 0.5)^{\mathrm{T}}$ for which the initial and boundary conditions are obtained from the analytical solution (38). Again the computational mesh consists of 32×32 patches. Note that for the considered circular domain, the curved geometry is recovered using the approach based on four rational quadratic segments presented in[24] among others. Thus, for the Burgers' equations in the circular domain, the bases are rational and quadratic in each parametric direction and the knot vectors are given by

$$\Xi^1 = \Big\{0, 0, 0, 1, 1, 1\Big\}, \qquad \Xi^2 = \Big\{0, 0, 0, 1, 1, 1\Big\}.$$

The corresponding control points and weights for the unit circle centered at $(0.5, 0.5)$ are listed in Table 4. In Figure 5 we display the numerical results for the solution $u$ obtained at time $t = 1$ for three different Reynolds numbers $Re = 10^2$, $10^4$ and $10^8$ using three NURBS degrees $p = 2$, 3 and 4. For comparison reasons, analytical results are also included in this figure. It is clear that for relatively small Reynolds numbers ($Re = 10^2$ and $Re = 10^4$) no significant differences between quadratic, cubic and quartic

**TABLE 2** Results for Example 2 obtained using different meshes and NURBS degrees for two Reynolds numbers $Re = 10^2$ and $Re = 10^3$ at time $t = 1$.

| | | $Re = 10^2$ | | | | $Re = 10^3$ | | | |
|---|---|---|---|---|---|---|---|---|---|
| $p$ | # patches | $L^1$-Error | Rate | $L^2$-Error | Rate | $L^1$-Error | Rate | $L^2$-Error | Rate |
| | 2×2 | 2.92823E-02 | — | 3.60456E-02 | — | 3.50042E-02 | — | 5.04156E-02 | — |
| | 4×4 | 1.51856E-02 | 0.9473 | 2.26892E-02 | 0.6678 | 2.08144E-02 | 0.7499 | 4.07903E-02 | 0.3056 |
| 1 | 8×8 | 5.61076E-03 | 1.4364 | 9.44974E-03 | 1.2637 | 1.10104E-02 | 0.9187 | 3.50227E-02 | 0.2199 |
| | 16×16 | 2.05832E-03 | 1.4467 | 3.71409E-03 | 1.3473 | 5.43884E-03 | 1.0175 | 1.76290E-02 | 0.9903 |
| | 32×32 | 7.32787E-04 | 1.4900 | 1.37643E-03 | 1.4321 | 1.90858E-03 | 1.5108 | 7.71762E-03 | 1.1917 |
| | 2×2 | 2.10443E-02 | — | 3.43412E-02 | — | 3.11002E-02 | — | 4.67234E-02 | — |
| | 4×4 | 1.00033E-02 | 1.0730 | 2.06245E-02 | 0.7356 | 1.53232E-02 | 1.0212 | 2.15173E-02 | 1.1186 |
| 2 | 8×8 | 4.45796E-03 | 1.1660 | 7.11201E-03 | 1.5360 | 7.16484E-03 | 1.0967 | 7.32788E-03 | 1.5540 |
| | 16×16 | 1.11417E-03 | 2.0004 | 1.64425E-03 | 2.1128 | 2.24528E-03 | 1.6740 | 1.78253E-03 | 2.0395 |
| | 32×32 | 2.10187E-04 | 2.4062 | 4.00432E-04 | 2.0378 | 4.22112E-04 | 2.4112 | 4.12567E-04 | 2.1112 |
| | 2×2 | 2.01213E-02 | — | 3.22019E-02 | — | 2.89482E-02 | — | 4.32090E-02 | — |
| | 4×4 | 9.93412E-03 | 1.0183 | 1.21344E-02 | 1.4080 | 1.22117E-02 | 1.2452 | 1.44712E-02 | 1.5781 |
| 3 | 8×8 | 4.31384E-03 | 1.2034 | 4.33762E-03 | 1.4841 | 4.49237E-03 | 1.4427 | 4.45210E-03 | 1.7006 |
| | 16×16 | 7.11417E-04 | 2.6002 | 1.00365E-03 | 2.1116 | 9.15286E-04 | 2.2952 | 1.16008E-03 | 1.9403 |
| | 32×32 | 8.26734E-05 | 3.1052 | 1.22322E-04 | 3.0365 | 9.94902E-05 | 3.2016 | 1.41611E-04 | 3.0342 |
| | 2×2 | 1.98056E-02 | — | 3.14227E-02 | — | 2.20211E-02 | — | 4.02114E-02 | — |
| | 4×4 | 9.55234E-03 | 1.0520 | 9.64118E-03 | 1.7045 | 9.78710E-03 | 1.1699 | 9.98733E-03 | 2.0094 |
| 4 | 8×8 | 2.30012E-03 | 2.0541 | 2.40123E-03 | 2.0054 | 2.45118E-03 | 1.9974 | 2.47154E-03 | 2.0147 |
| | 16×16 | 2.28201E-04 | 3.3333 | 2.30211E-04 | 3.3827 | 2.54034E-04 | 3.2704 | 2.60748E-04 | 3.2447 |
| | 32×32 | 1.26018E-05 | 4.1786 | 1.43812E-05 | 4.0007 | 1.30766E-05 | 4.2800 | 1.55671E-05 | 4.0661 |
| | 2×2 | 1.72109E-02 | — | 2.01327E-02 | — | 2.00472E-02 | — | 3.89743E-02 | — |
| | 4×4 | 9.01122E-03 | 0.9335 | 9.23423E-03 | 1.1245 | 9.31219E-03 | 1.1062 | 9.78812E-03 | 1.9934 |
| 5 | 8×8 | 1.55344E-03 | 2.5363 | 1.57514E-03 | 2.5515 | 1.78201E-03 | 2.3856 | 1.89615E-03 | 2.3680 |
| | 16×16 | 1.01422E-04 | 3.9370 | 1.02171E-04 | 3.9464 | 1.94216E-04 | 3.1978 | 1.98766E-04 | 3.2539 |
| | 32×32 | 3.04118E-06 | 5.0596 | 3.12334E-06 | 5.0318 | 6.01110E-06 | 5.0139 | 6.23102E-06 | 4.9955 |

solutions are observed. Indeed the three numerical solutions are in good agreement with the exact solution. This can be related to the relatively small values of the Reynolds numbers which result in smooth solutions. At the high Reynolds number $Re = 10^8$, the quadratic and cubic NURBS fail to produce good results and only the quartic result matches the analytical solution. Note that for the case with $Re = 10^8$, the computational solution develop a strong shock which can not be captured by NURBS of low degrees. To further highlight the effect of the $k$-refinement on the numerical solutions for this example, we present in Figure 6 the cross-sections of the numerical solutions at the main diagonal $y = 1 - x$ using $p = 2$, 3 and 4 at two different instants $t = 0.5$ and $t = 1$. No significant differences are observed at time $t = 0.5$ using $Re = 10^2$. However, when advancing in time, the numerical dissipation becomes visible in the quadratic and cubic solutions and the shock location is shifted compared to the exact solution. Again, the NURBS of quadratic and cubic orders are clearly not enough to maintain the stability of the computed solutions as spurious oscillations appear in the shock areas when high Reynolds numbers are considered, compare the results obtained for $Re = 10^8$ in Figure 6. From the same results we can confirm that the NURBS of quartic order are suitable to capture the sharp gradients in the solutions and produce satisfactory results.

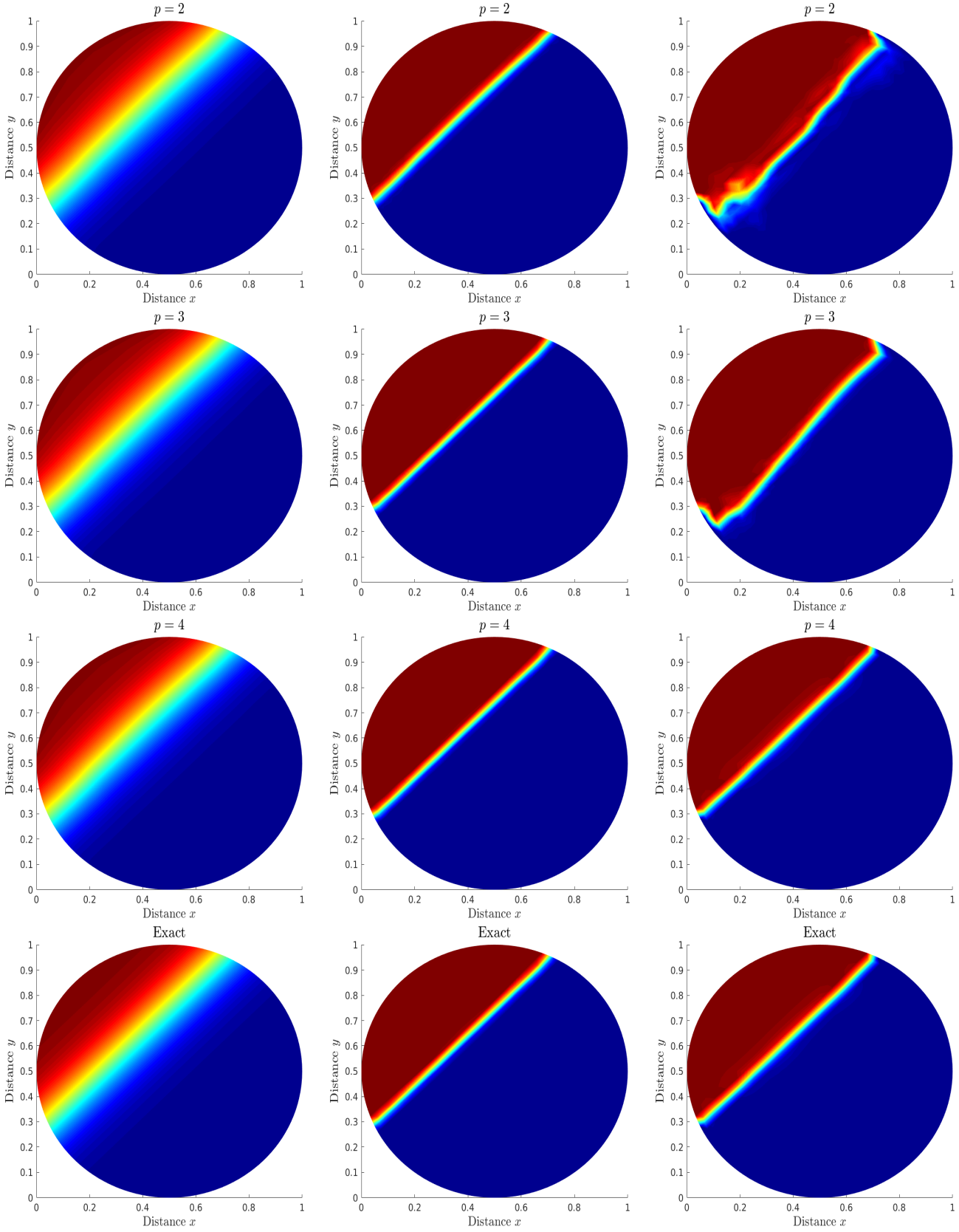


**FIGURE 5** Results for the solution $u$ in Example 2 at time $t = 1$ obtained using a mesh of $32 \times 32$ elements with $p = 2$ (first row), $p = 3$ (second row), $p = 4$ (third row) and the exact solution (fourth row). Here, $Re = 10^2$ (first column), $Re = 10^4$ (second column) and $Re = 10^8$ (third column).

**TABLE 3** Results for Example 2 obtained using different meshes and NURBS degrees for two Reynolds numbers $Re = 10^4$ and $Re = 10^5$ at time $t = 1$.

| | | $Re = 10^4$ | | | | $Re = 10^5$ | | | |
|---|---|---|---|---|---|---|---|---|---|
| $p$ | # patches | $L^1$-Error | Rate | $L^2$-Error | Rate | $L^1$-Error | Rate | $L^2$-Error | Rate |
| 1 | 2×2 | 3.77514E-02 | — | 5.44018E-02 | — | 3.79701E-02 | — | 5.48730E-02 | — |
| | 4×4 | 2.29547E-02 | 0.7177 | 4.42486E-02 | 0.2980 | 2.31434E-02 | 0.7143 | 4.46592E-02 | 0.2971 |
| | 8×8 | 1.23423E-02 | 0.8952 | 4.22031E-02 | 0.0683 | 1.74666E-02 | 0.4060 | 4.23513E-02 | 0.0766 |
| | 16×16 | 6.13404E-03 | 1.0087 | 2.49374E-02 | 0.7590 | 8.70146E-03 | 1.0053 | 2.74143E-02 | 0.6275 |
| | 32×32 | 2.93302E-03 | 1.0645 | 1.63361E-02 | 0.6102 | 4.27672E-03 | 1.0248 | 1.81790E-02 | 0.5927 |
| 2 | 2×2 | 3.54916E-02 | — | 5.31807E-02 | — | 3.50481E-02 | — | 5.31680E-02 | — |
| | 4×4 | 1.54345E-02 | 1.2013 | 2.34005E-02 | 1.1844 | 1.62733E-02 | 1.1068 | 2.42771E-02 | 1.1310 |
| | 8×8 | 7.39987E-03 | 1.0606 | 7.45661E-03 | 1.6499 | 7.44587E-03 | 1.1280 | 7.60211E-03 | 1.6751 |
| | 16×16 | 2.70011E-03 | 1.4545 | 2.75093E-03 | 1.4386 | 2.84321E-03 | 1.3889 | 2.82105E-03 | 1.4307 |
| | 32×32 | 6.01315E-04 | 2.1668 | 6.25344E-04 | 2.1372 | 6.21406E-04 | 2.1939 | 6.30219E-04 | 2.1623 |
| 3 | 2×2 | 3.32702E-02 | — | 5.11754E-02 | — | 3.42119E-02 | — | 5.16232E-02 | — |
| | 4×4 | 1.33839E-02 | 1.3137 | 1.97307E-02 | 1.3750 | 1.46655E-02 | 1.2221 | 1.99659E-02 | 1.3705 |
| | 8×8 | 4.57091E-03 | 1.5499 | 4.66211E-03 | 2.0814 | 4.62120E-03 | 1.6661 | 4.78012E-03 | 2.0624 |
| | 16×16 | 9.73823E-04 | 2.2307 | 9.83012E-04 | 2.2457 | 9.80091E-04 | 2.2373 | 9.92167E-04 | 2.2684 |
| | 32×32 | 9.98013E-05 | 3.2865 | 9.99875E-05 | 3.2974 | 9.99788E-05 | 3.2932 | 1.09213E-04 | 3.1834 |
| 4 | 2×2 | 3.11324E-02 | — | 5.00234E-02 | — | 3.31004E-02 | — | 5.02145E-02 | — |
| | 4×4 | 9.94301E-03 | 1.6467 | 9.98765E-03 | 2.3244 | 9.97865E-03 | 1.7299 | 1.78944E-02 | 1.4886 |
| | 8×8 | 2.61002E-03 | 1.9296 | 2.68010E-03 | 1.8979 | 2.73112E-03 | 1.8694 | 2.73201E-03 | 2.7115 |
| | 16×16 | 2.70114E-04 | 3.2724 | 2.78389E-04 | 3.2671 | 2.84503E-04 | 3.2630 | 2.82251E-04 | 3.2749 |
| | 32×32 | 1.55845E-05 | 4.1154 | 1.69455E-05 | 4.0381 | 1.68219E-05 | 4.0800 | 1.77003E-05 | 3.9951 |
| 5 | 2×2 | 2.93365E-02 | — | 4.87946E-02 | — | 3.21201E-02 | — | 4.89482E-02 | — |
| | 4×4 | 9.44181E-03 | 1.6356 | 9.90692E-03 | 2.3002 | 9.54210E-03 | 1.7511 | 9.95722E-03 | 2.2974 |
| | 8×8 | 1.91921E-03 | 2.2986 | 1.98845E-03 | 2.3168 | 1.98477E-03 | 2.2653 | 1.99840E-03 | 2.3169 |
| | 16×16 | 2.02114E-04 | 3.2473 | 2.43289E-04 | 3.0309 | 2.23125E-04 | 3.1530 | 2.48655E-04 | 3.0066 |
| | 32×32 | 6.32128E-06 | 4.9988 | 7.27206E-06 | 5.0642 | 6.97981E-06 | 4.9985 | 7.75788E-06 | 5.0023 |

## 4.3 | Example 3

Our final example consists of solving the Burgers' system (1) in an L-shape computational domain defined by $\Omega = [-2, 2] \times [-2, 2] \backslash [0, 2] \times [0, 2]$ subject to initial and Dirichlet boundary conditions obtained from the following analytical solution

$$\begin{aligned} u(x, y, t) &= -\frac{4\pi \exp\left(-\frac{5\pi^2 t}{Re}\right) \cos(2\pi x) \sin(\pi y)}{Re\left(2 + \exp\left(-\frac{5\pi^2 t}{Re}\right) \sin(2\pi x) \sin(\pi y)\right)}, \\ v(x, y, t) &= -\frac{2\pi \exp\left(-\frac{5\pi^2 t}{Re}\right) \sin(2\pi x) \cos(\pi y)}{Re\left(2 + \exp\left(-\frac{5\pi^2 t}{Re}\right) \sin(2\pi x) \sin(\pi y)\right)}. \end{aligned} \tag{39}$$

A similar geometry has been considered in[45] among others. This problem has also been widely used in the literature to analyze the performance of numerical methods for solving coupled Burgers' equations, see for instance[20,18]. A uniform mesh with 512 squared patches and patch side length $h = 0.042$ is used in our simulations. As in the previous test examples, the $k$-refinement

**TABLE 4** Control points and weights used in the quadrature formula for a unit circle centered at (0.5, 0.5).

| i | $B_i$ | $\omega_i$ |
|---|---|---|
| 1 | (0.1464, 0.1464) | 1 |
| 2 | (0.5000, 0.0000) | $1/\sqrt{2}$ |
| 3 | (0.8536, 0.1464) | 1 |
| 4 | (0.0000, 0.5000) | $1/\sqrt{2}$ |
| 5 | (0.5000, 0.5000) | 1 |
| 6 | (1.0000, 0.5000) | $1/\sqrt{2}$ |
| 7 | (0.1464, 0.8536) | 1 |
| 8 | (0.5000, 1.0000) | $1/\sqrt{2}$ |
| 9 | (0.8536, 0.8536) | 1 |

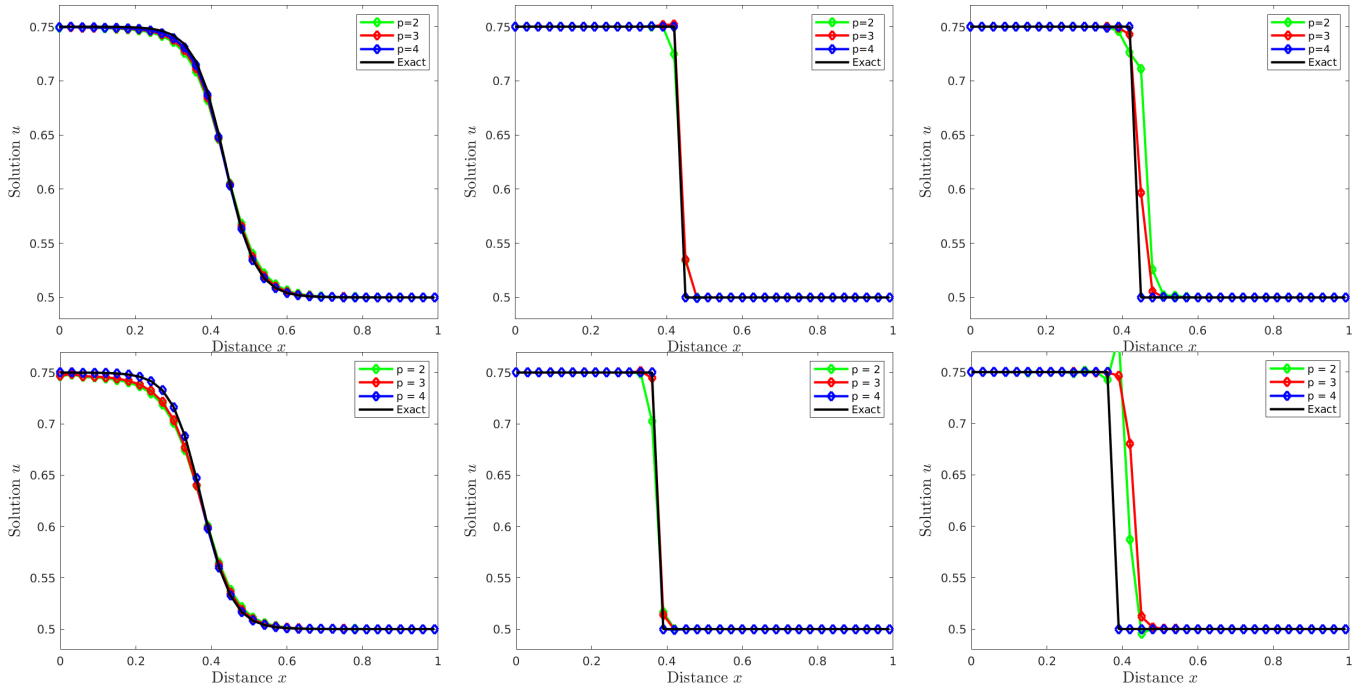


**FIGURE 6** Cross-sections at the diagonal $y = 1 - x$ of the solution $u$ obtained for Example 2 at time $t = 0.5$ (top) and $t = 1$ (bottom) on a mesh of $32 \times 32$ elements using different NURBS degrees for $Re = 10^2$ (left plot), $Re = 10^4$ (middle plot) and $Re = 10^8$ (right plot).

method is used for refinements and numerical results are presented for the solution component $u$ using different degrees $p$ at four different Reynolds numbers.

In Figure 7 we display the results of the solution $u$ using $p = 1$, 3 and 5 at time $t = 1$ for two different Reynold numbers $Re = 10$ and $Re = 10^3$. Note that for this example, the solutions (39) vanish when the Reynolds number reaches high values. The clear indication from Figure 7 is that the numerical diffusion is clearly visible in the results obtained using linear polynomials ($p = 1$) for both Reynolds numbers $Re = 10$ than $Re = 10^3$. From the same figure, the numerical solutions obtained using the

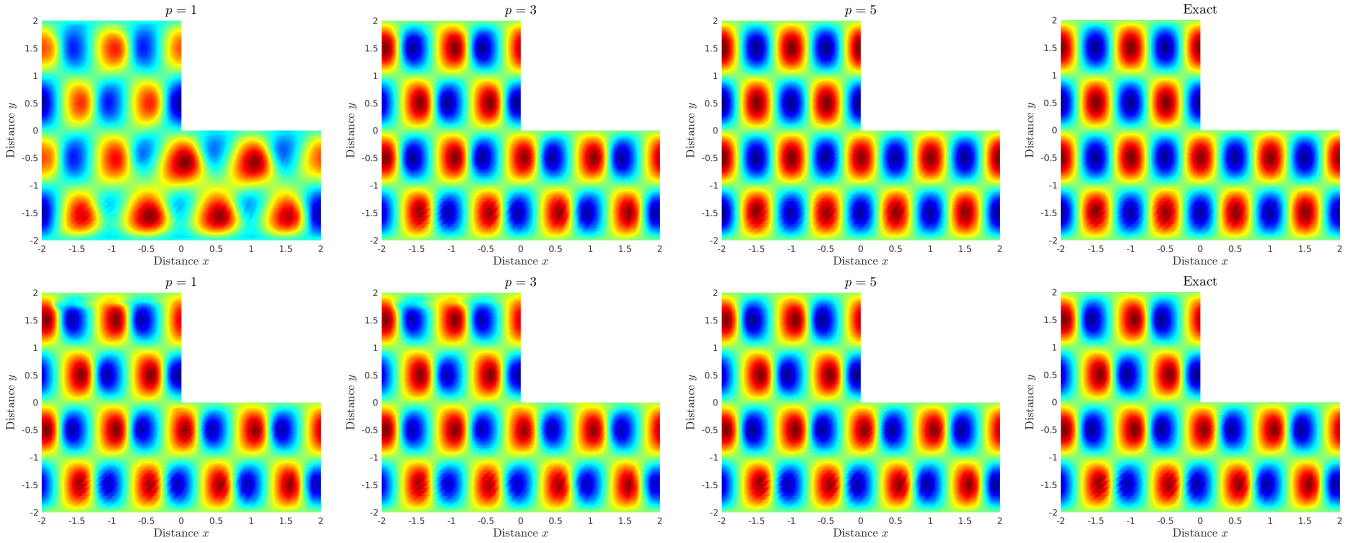


**FIGURE 7** Results for the solution $u$ in Example 3 at time $t = 1$ obtained using a mesh of 512 elements with $p = 2$ (first column), $p = 3$ (second column), $p = 4$ (third column) and the exact solution (fourth column). Here, $Re = 10$ (first row) and $Re = 10^3$ (second row).

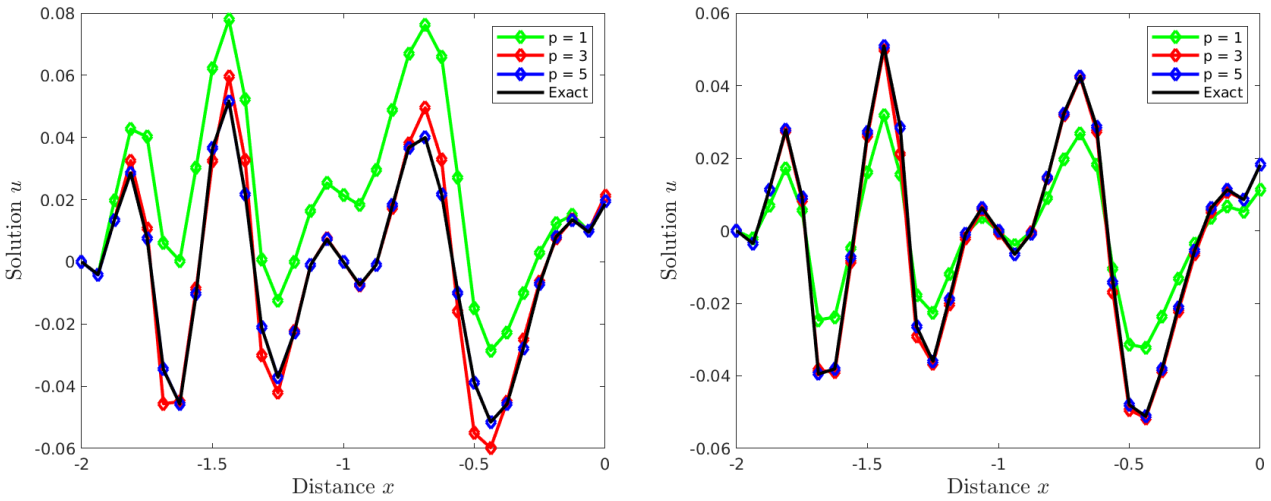


**FIGURE 8** Cross-sections at the diagonal $y = x$ of the solution $u$ obtained for Example 3 at time $t = 1$ on a mesh of 512 elements using different NURBS degrees for $Re = 10$ (left plot) and $Re = 10^3$ (right plot).

cubic polynomials reduce this numerical dissipation and those results obtained using the quintic polynomials appear to provide the most accurate results compared to the analytical solutions. To further demonstrate these features for this test example, cross-sections of these solutions along the main diagonal $y = x$ are shown in Figure 8. It is clear that the linear NURBS fail to resolve this test example at the considered Reynolds numbers whereas, the NURBS of cubic and quintic orders accurately capture the features of the numerical solutions. No visible differences have been detected in Figure 8 for the results obtained NURBS of quintic order and analytical solutions.

To quantify the errors for this example, we present in Table 5 the $L^1$-error and the corresponding convergence rates using four different Reynolds numbers and different NURBS orders. It is evident that, fixing the polynomial order and refining the mesh using $h$-refinement results in a decay of all errors and as expected, the optimal convergence rates are also achieved for the selected NURBS orders at all considered Reynolds numbers $Re = 10$, $Re = 10^2$, $Re = 10^3$ and $Re = 10^4$. It should also be

**TABLE 5** Results for Example 3 obtained using different meshes and NURBS degrees for four Reynolds numbers $Re = 10$, $Re = 10^2$, $Re = 10^3$ and $Re = 10^4$ at time $t = 1$.

| | | $Re = 10$ | | $Re = 10^2$ | | $Re = 10^3$ | | $Re = 10^4$ | |
|---|---|---|---|---|---|---|---|---|---|
| $p$ | # patches | $L^1$-Error | Rate | $L^1$-Error | Rate | $L^1$-Error | Rate | $L^1$-Error | Rate |
| | 2×2 | 1.97185E+00 | — | 1.62819E+01 | — | 2.43326E+00 | — | 1.46467E-01 | — |
| | 4×4 | 1.04903E+00 | 0.9105 | 8.27898E+00 | 0.9757 | 1.13638E+00 | 1.0984 | 6.38093E-02 | 1.1987 |
| 1 | 8×8 | 5.20114E-01 | 1.0122 | 3.62096E+00 | 1.1931 | 5.19759E-01 | 1.1285 | 2.77441E-02 | 1.2016 |
| | 16×16 | 2.50768E-01 | 1.0525 | 1.58653E+00 | 1.1905 | 2.35802E-01 | 1.1403 | 8.75626E-03 | 1.6638 |
| | 32×32 | 7.68309E-02 | 1.7066 | 5.31663E-01 | 1.5773 | 1.03409E-01 | 1.1892 | 2.70506E-03 | 1.6947 |
| | 2×2 | 1.83075E+00 | — | 1.44829E+01 | — | 1.51168E+00 | — | 1.21442E-01 | — |
| | 4×4 | 8.73670E-01 | 1.0673 | 3.59189E+00 | 2.0115 | 3.56541E-01 | 2.0840 | 2.91737E-02 | 2.0575 |
| 2 | 8×8 | 1.90416E-01 | 2.1979 | 5.30333E-01 | 2.7598 | 8.13758E-02 | 2.1314 | 6.66073E-03 | 2.1309 |
| | 16×16 | 3.99399E-02 | 2.2533 | 6.75898E-02 | 2.9720 | 1.37134E-02 | 2.5690 | 1.49639E-03 | 2.1542 |
| | 32×32 | 7.54893E-03 | 2.4035 | 8.89929E-03 | 2.9250 | 1.98022E-03 | 2.7919 | 3.32916E-04 | 2.1683 |
| | 2×2 | 8.69466E-01 | — | 6.32981E+00 | — | 9.99346E-01 | — | 8.54428E-02 | — |
| | 4×4 | 1.65846E-01 | 2.3903 | 8.68885E-01 | 2.8649 | 1.10091E-01 | 3.1823 | 1.60801E-02 | 2.4097 |
| 3 | 8×8 | 1.83075E-02 | 3.1793 | 9.87625E-02 | 3.1371 | 1.09701E-02 | 3.3270 | 1.87336E-03 | 3.1016 |
| | 16×16 | 1.91796E-03 | 3.2548 | 1.05026E-02 | 3.3232 | 1.02664E-03 | 3.4176 | 2.01857E-04 | 3.2142 |
| | 32×32 | 1.55222E-04 | 3.6272 | 1.03141E-03 | 3.3480 | 9.50853E-05 | 3.4326 | 2.14757E-05 | 3.2326 |
| | 2×2 | 7.82473E-01 | — | 5.47265E+00 | — | 8.00651E-01 | — | 6.49480E-02 | — |
| | 4×4 | 9.52567E-02 | 3.0381 | 6.34125E-01 | 3.1094 | 4.81531E-02 | 4.0555 | 5.43134E-03 | 3.5799 |
| 4 | 8×8 | 9.21164E-03 | 3.3703 | 3.62189E-02 | 4.1300 | 2.61681E-03 | 4.2017 | 3.33107E-04 | 4.0273 |
| | 16×16 | 5.56703E-04 | 4.0485 | 2.04925E-03 | 4.1436 | 1.35048E-04 | 4.2763 | 2.02092E-05 | 4.0429 |
| | 32×32 | 3.20051E-05 | 4.1205 | 1.06476E-04 | 4.2665 | 7.00511E-06 | 4.2689 | 1.20457E-06 | 4.0684 |
| | 2×2 | 7.11369E-01 | — | 4.94090E+00 | — | 6.67355E-01 | — | 4.81706E-02 | — |
| | 4×4 | 8.11106E-02 | 3.1326 | 5.64757E-01 | 3.1291 | 2.05435E-02 | 5.0217 | 1.47014E-03 | 5.0341 |
| 5 | 8×8 | 9.60609E-03 | 3.0779 | 2.80919E-02 | 4.3294 | 6.12976E-04 | 5.0667 | 4.28819E-05 | 5.0994 |
| | 16×16 | 7.90226E-04 | 3.6036 | 8.34701E-04 | 5.0727 | 1.60181E-05 | 5.2581 | 1.25041E-06 | 5.0999 |
| | 32×32 | 2.43422E-05 | 5.0207 | 2.26406E-05 | 5.2043 | 4.67311E-07 | 5.0992 | 3.38080E-08 | 5.2089 |

pointed out that a slow decay in the computed errors is detected in the results obtained at $Re = 10$ using the quintic NURBS. Similar remarks have been observed for results obtained using the $L^2$-error and not reported here for brevity. Note that, the proposed isogeometric modified method of characteristics is typically designed to solve this class of convection-dominated flow problems using time steps ten to twenty times larger than its Eulerian counterparts. It should also be stressed that the performance of the proposed isogeometric modified method of characteristics is very attractive since the computed solutions remain stable and highly accurate even when coarse meshes and high Reynolds numbers are used without requiring nonlinear solvers or small time steps to be taken in the simulations.

## 5 | CONCLUDING REMARKS

A novel isogeometric modified method of characteristics has been investigated for numerical solution of the two-dimensional coupled Burgers' equations. The proposed method exploits the interesting features offered by both techniques the modified method of characteristics and the high-order NURBS elements to construct a highly accurate algorithm for the numerical treatment of nonlinear convection-dominated problems. The main advantage of the new method is that, the nonlinear convective term that has to be treated carefully in most of Eulerian-based finite element methods has been removed from the new method by using the modified method of characteristics to interpret the transport nature of the governing equations. This has also

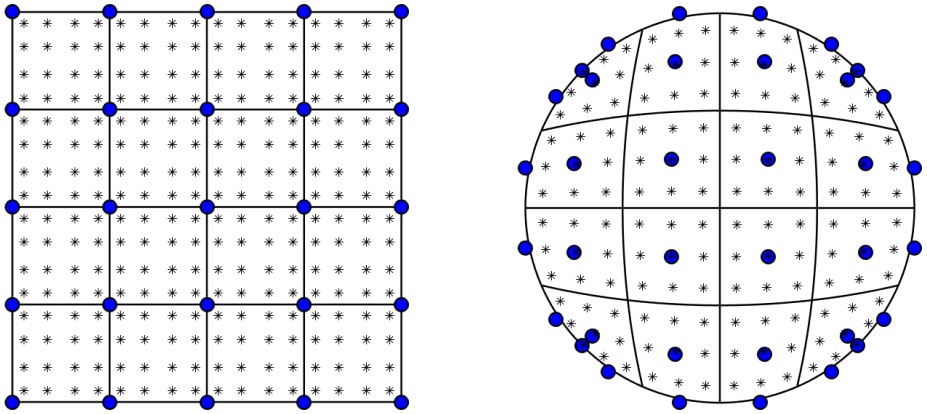

**FIGURE 9** Distribution of $3 \times 3$ Gauss-Jacobi nodes in a mesh with $4 \times 4$ patches for linear space in a squared domain (left plot) and quadratic space in a circular domain (right plot).

allowed for large time steps to be used in the simulations resulting in a reduction for the computational costs. The time integration has been carried out using a third-order explicit Runge-Kutta scheme. To demonstrate the computational efficiency of the novel method, we have considered two-dimensional coupled Burgers' equations in both regular and complex geometries. Problems with known analytical solutions have been selected to illustrate the accuracy, robustness and performance of the proposed method. It has been shown that the proposed isogeometric modified method of characteristics enjoys the computational advantages and achieves accurate solutions for high Reynolds numbers up to $Re = 10^8$. Furthermore, the computed results support our expectations for a stable and highly accurate isogeometric finite element method for two dimensional nonlinear coupled Burgers' equations. This fact, as well as its favorable stability properties, make it an attractive alternative for flow solvers based on finite element discretizations. Future work will concentrate on developing high-order time integration schemes for isogeometric modified method of characteristics and extension of these techniques to incompressible Navier-Stokes equations in the primitive variables. It is worth noting that developing an isogeometric analysis modified method of characteristics for solving the incompressible Navier-Stokes equations is not trivial for several reasons. First, the presence of the pressure in the equations with no evolution for its dynamics requires special treatment such as the projection methods. Second, the incompressibility condition of the flow needs to be satisfied for the isogeometric discretized systems. Third, stabilized finite element methods for the incompressible Navier-Stokes equations are needed to be in the mixed form since the unified finite element methods do not in general satisfy the discrete inf-sup condition. This would require that the finite element space for the pressure should be one degree less than the space for the velocity and this should also be achieved using the NURBS basis functions.

□

# APPENDIX

## A GAUSS-JACOBI QUADRATURE RULES

Consider a smooth function $f$ on the domain $[-1, 1]$. The Gauss-Jacobi rule implemented in the present study is defined as

$$\int_{-1}^{1} (1 - \boldsymbol{x})^{\alpha} (1 + \boldsymbol{x})^{\beta} f(\boldsymbol{x}) d\boldsymbol{x} = \sum_{g=1}^{N_g} w_g f(\boldsymbol{x}_g) + \epsilon, \tag{A1}$$

where $\alpha$ and $\beta$ are real exponents, $N_g$ is the total number of quadrature points used, and $\epsilon$ is the error term, see for instance[36]. The weights $w_g$ are given by

$$w_g = -\frac{2N_g+\alpha+\beta+2}{2N_g+\alpha+\beta+1}\frac{\gamma(N_g+\beta+1)\gamma(N_g+\alpha+\beta+1)}{(N_g+1)!\gamma(N_g+\alpha+\beta+1)}\frac{2^{\alpha+\beta}}{P_{N_g}^{(\alpha+\beta)'}(\boldsymbol{x}_g)P_{N_g+1}^{(\alpha+\beta)}(\boldsymbol{x}_g)}, \tag{A2}$$

where $\gamma$ denotes the $\gamma$-function given by $\gamma(N_g) = (N_g - 1)!$. The series form of Jacobi polynomials $P^{(\alpha,\beta)}$ are defined by[46]

$$P^{(\alpha,\beta)}(\boldsymbol{x}) = \frac{1}{2^{N_g}}\sum_{i=0}^{[N_g/2]}\binom{N_g+\alpha}{i}\binom{N_g+\beta}{N_g-i}(\boldsymbol{x}-1)^{N_g-i}(\boldsymbol{x}+1)^i. \tag{A3}$$

The error term $\epsilon^{N_g}$ in the $N_g$-points rule is given by

$$\epsilon^{N_g} = \frac{\gamma(N_g+\alpha+1)\gamma(N_g+\beta+1)\gamma(N_g+\alpha+\beta+1)}{(2N_g+\alpha+\beta+1)[\gamma(2N_g+\alpha+\beta+1)]^2}\frac{N_g!2^{2N_g+\alpha+\beta+1}}{(2N_g)!}f^{2N_g}(\zeta), \qquad \zeta\in(-1,1). \tag{A4}$$

In a special case, the above rule is reduced to the Gauss-Legendre quadrature for $\alpha = \beta = 0$ and for $\alpha = \beta = \pm\frac{1}{2}$ it results in the Chebyshev quadrature rule. An illustration of $4\times4$ Gauss-Jacobi nodes in a mesh with $4\times4$ patches for the linear space in a squared domain is depicted in the left plot of Figure 9. For the quadratic space in a circular domain, an illustration of $3\times3$ quadrature nodes is shown in the right plot of Figure 9.

## References


1. Discacciati N, Hesthaven J, Ray D. Controlling oscillations in high-order Discontinuous Galerkin schemes using artificial viscosity tuned by neural networks. *Journal of Computational Physics* 2020: 109304.
2. Li R, Wu Q, Zhu S. Proper orthogonal decomposition with SUPG-stabilized isogeometric analysis for reduced order modelling of unsteady convection-dominated convection-diffusion-reaction problems. *Journal of Computational Physics* 2019; 387: 280–302.
3. John V, Schumacher L. A study of isogeometric analysis for scalar convection–diffusion equations. *Applied Mathematics Letters* 2014; 27: 43–48.
4. Langer U, Moore S, Neumüller M. Space–time isogeometric analysis of parabolic evolution problems. *Computer methods in applied mechanics and engineering* 2016; 306: 342–363.
5. Dhawan S, Kapoor S, Kumar S. Numerical method for advection diffusion equation using FEM and B-splines. *Journal of Computational Science* 2012; 3(5): 429–437.
6. Wu M, Wang Y, Mourrain B, Nkonga B, Cheng C. Convergence rates for solving elliptic boundary value problems with singular parameterizations in isogeometric analysis. *Computer Aided Geometric Design* 2017; 52: 170–189.
7. Łoś M, Muñoz-Matute J, Muga I, Paszyński M. Isogeometric Residual Minimization Method (IGRM) with direction splitting for non-stationary advection–diffusion problems. *Computers & Mathematics with Applications* 2020; 79(2): 213–229.
8. Prenter dF, Verhoosel C, Brummelen vE. Preconditioning immersed isogeometric finite element methods with application to flow problems. *Computer Methods in Applied Mechanics and Engineering* 2019; 348: 604–631.
9. Jaeschke A, Möller M. High-Order Isogeometric Methods for Compressible Flows. In: Springer. 2020 (pp. 21–29).
10. Manni C, Pelosi F, Sampoli M. Isogeometric analysis in advection–diffusion problems: Tension splines approximation. *Journal of Computational and Applied Mathematics* 2011; 236(4): 511–528.
11. Buffa A, Falco dC, Sangalli G. Isogeometric analysis: stable elements for the 2D Stokes equation. *International Journal for Numerical Methods in Fluids* 2011; 65(11-12): 1407–1422.

12. Bressan A, Sangalli G. Isogeometric discretizations of the Stokes problem: stability analysis by the macroelement technique. *IMA Journal of Numerical Analysis* 2013; 33(2): 629–651.

13. Bressan A. Isogeometric regular discretization for the Stokes problem. *IMA journal of numerical analysis* 2011; 31(4): 1334–1356.

14. Evans J, Hughes T. Isogeometric divergence-conforming B-splines for the unsteady Navier–Stokes equations. *Journal of Computational Physics* 2013; 241: 141–167.

15. Tagliabue A, Dede L, Quarteroni A. Isogeometric analysis and error estimates for high order partial differential equations in fluid dynamics. *Computers & Fluids* 2014; 102: 277–303.

16. Bulling J, John V, Knobloch P. Isogeometric analysis for flows around a cylinder. *Applied Mathematics Letters* 2017; 63: 65–70.

17. Hosseini B, Möller M, Turek S. Isogeometric analysis of the Navier–Stokes equations with Taylor–Hood B-spline elements. *Applied Mathematics and Computation* 2015; 267: 264–281.

18. Liao W. A fourth-order finite-difference method for solving the system of two-dimensional Burgers' equations. *International journal for numerical methods in fluids* 2010; 64(5): 565–590.

19. Kannan R, Wang Z. A high order spectral volume solution to the Burgers' equation using the Hopf–Cole transformation. *International journal for numerical methods in fluids* 2012; 69(4): 781–801.

20. Ngondiep E. An efficient three-level explicit time-split scheme for solving two-dimensional unsteady nonlinear coupled Burgers' equations. *International Journal for Numerical Methods in Fluids* 2020; 92(4): 266–284.

21. Shi F, Zheng H, Cao Y, Li J, Zhao R. A fast numerical method for solving coupled Burgers' equations. *Numerical Methods for Partial Differential Equations* 2017; 33(6): 1823–1838.

22. El-Amrani M, Seaid M. A finite element semi-Lagrangian method with $L^2$ interpolation. *Int. J. Numer. Meth. Engng.* 2012; 90(12): 1485–1507.

23. El-Amrani M, Seaid M. An Lˆ2-Projection for the Galerkin-Characteristic Solution of Incompressible Flows. *SIAM Journal on Scientific Computing* 2011; 33(6): 3110–3131.

24. Hughes T, Cottrell J, Bazilevs Y. Isogeometric analysis: CAD, finite elements, NURBS, exact geometry and mesh refinement. *Computer methods in applied mechanics and engineering* 2005; 194(39-41): 4135–4195.

25. Nguyen V, Anitescu C, Bordas S, Rabczuk T. Isogeometric analysis: an overview and computer implementation aspects. *Mathematics and Computers in Simulation* 2015; 117: 89–116.

26. Cottrell J, Hughes T, Bazilevs Y. *Isogeometric analysis: toward integration of CAD and FEA*. John Wiley & Sons . 2009.

27. Piegl L, Tiller W. *The NURBS book*. Springer Science & Business Media . 2012.

28. Bazilevs Y, Veiga dL, Cottrell J, Hughes T, Sangalli G. Isogeometric analysis: approximation, stability and error estimates for h-refined meshes. *Mathematical Models and Methods in Applied Sciences* 2006; 16(07): 1031–1090.

29. Lipton S, Evans J, Bazilevs Y, Elguedj T, Hughes T. Robustness of isogeometric structural discretizations under severe mesh distortion. *Computer Methods in Applied Mechanics and Engineering* 2010; 199(5-8): 357–373.

30. Shu C. Total Variation Diminishing Time Discretizations. *SIAM J. Sci. Stat. Comput.* 1988; 9: 1073–1084.

31. Allievi A, Bermejo R. A generalized particle search–locate algorithm for arbitrary grids. *Journal of Computational Physics* 1997; 132(2): 157–166.

32. Xu K, Darve E. Isogeometric collocation method for the fractional Laplacian in the 2D bounded domain. *Computer Methods in Applied Mechanics and Engineering* 2020; 364: 112936.

33. Schillinger D, Hossain S, Hughes T. Reduced Bézier element quadrature rules for quadratic and cubic splines in isogeometric analysis. *Computer Methods in Applied Mechanics and Engineering* 2014; 277: 1–45.

34. Bartoň M, Calo V. Gauss–Galerkin quadrature rules for quadratic and cubic spline spaces and their application to isogeometric analysis. *Computer-Aided Design* 2017; 82: 57–67.

35. Hale N, Townsend A. Fast and accurate computation of Gauss–Legendre and Gauss–Jacobi quadrature nodes and weights. *SIAM Journal on Scientific Computing* 2013; 35(2): A652–A674.

36. Chernov A, Schwab C. Exponential convergence of Gauss–Jacobi quadratures for singular integrals over simplices in arbitrary dimension. *SIAM Journal on Numerical Analysis* 2012; 50(3): 1433–1455.

37. Rathod H, Venkatesudu B, Nagaraja K, M.D.S. Islam M. Gauss Legendre–Gauss Jacobi quadrature rules over a tetrahedral region. *Applied mathematics and computation* 2007; 190(1): 186–194.

38. Gil A, Segura J, Temme N. Fast and reliable high-accuracy computation of Gauss–Jacobi quadrature. *Numerical Algorithms* 2020: 1–29.

39. Sastre dP, Bermejo R. Error analysis for hp-FEM semi-Lagrangian second order BDF method for convection-dominated diffusion problems. *Journal of Scientific Computing* 2011; 49(2): 211–237.

40. Mirbagheri Y, Nahvi H, Parvizian J, Düster A. Reducing spurious oscillations in discontinuous wave propagation simulation using high-order finite elements. *Computers & Mathematics with Applications* 2015; 70(7): 1640–1658.

41. Si Z, Wang J, Sun W. Unconditional stability and error estimates of modified characteristics FEMs for the Navier–Stokes equations. *Numerische Mathematik* 2016; 134(1): 139–161.

42. Wang J, Si Z, Sun W. A new error analysis of characteristics-mixed FEMs for miscible displacement in porous media. *SIAM Journal on Numerical Analysis* 2014; 52(6): 3000–3020.

43. Lentine M, Grétarsson J, Fedkiw R. An unconditionally stable fully conservative semi-Lagrangian method. *Journal of computational physics* 2011; 230(8): 2857–2879.

44. Veiga L, Rivas ABJ, Sangalli G. Some estimates for h–p–k-refinement in Isogeometric Analysis. *Numerische Mathematik* 2011; 118(2): 271–305.

45. Dosiyev A, Mazhar Z, Buranay S. Block method for problems on L-shaped domains. *Journal of computational and applied mathematics* 2010; 235(3): 805–816.

46. Kythe P, Schäferkotter M. *Handbook of computational methods for integration*. CRC Press . 2004.